UNIVERSIDADE DE LISBOA
FACULDADE DE CIÊNCIAS
DEPARTAMENTO DE BIOLOGIA VEGETAL

Voltage-Gated Potassium Currents of the Trigeminal Ganglion – Relevance to Chronic Orofacial Pain

Ana Rosa Maço Abreu

Mestrado em Biologia Molecular e Genética

Dissertação orientada por:
Professora Doutora Maria Margarida Perestrello Ramos
Professor Doutor Pedro Afonso dos Santos Baltazar de Lima

2017

ACKNOWLEDGEMENTS

Ao Doutor Pedro Lima por me acolher no laboratório, por me orientar e por me apresentar ao inesperadamente fascinante mundo da eletrofisiologia.

A todo o pessoal da Sea4Us por me receberem, pela boa disposição e por terem paciência tanto para o meu silêncio como as situações em que ele era preferível.

Às minhas colegas/tutoras, Joana e Beatriz, por me ensinarem grande parte do muito que aprendi este ano e por me ajudarem a crescer, não só enquanto cientista, mas também como pessoa.

À Joana pelo empurrão para fora da minha pequena zona de conforto que foi o impulsionador de tudo o resto e pelas perguntas difíceis que me obrigaram a seguir em frente, à procura de soluções para problemas que eu nem sabia que tinha. Por muito que me custe admitir, obrigada por tornares as casuais frustrações do patch clamp menos frustrantes com os episódios da *Rosanovela*.

À Beatriz, sem quem nada disto teria sido possível, pelo incrível apoio técnico ao longo de todo o ano, com especial destaque para todo o trabalho e paciência por trás do modelo de dor. Obrigada pelas bolachas, pelo entusiasmo contagiante, pelas piadas hilariantes e pela paciência para as minhas não tão hilariantes tentativas. Mas principalmente obrigada por acreditares em mim.

A todos os meus amigos não só por aturaram as minhas crises existenciais, mas também por agirem como se elas fizessem sentido. Obrigada pelo apoio e pela energia positiva, muitas vezes enviada à distância. Um agradecimento especial às minhas colegas de casa pelo apoio emocional do último ano.

À minha família pelo apoio incondicional em todas as frentes e durante todo o meu percurso.

À minha irmã pela paciência e pelas fotos dos gatos nas semanas longe de casa. Obrigada por estares do meu lado nas lutas contra o Illustrator.

Em especial o maior agradecimento à minha mãe por fazer das tripas coração de forma a garantir que eu possa sempre seguir o meu. Obrigada por seres a minha rede de segurança.

Por fim, um agradecimento às entidades financiadoras: Sea4Us, CRESC Algarve 2020, Lisboa 2020, Portugal 2020 e União Europeia através dos Fundos Europeus Estruturais e de Investimento.

RESUMO

A sobrevivência de um organismo depende em grande parte da sua capacidade de perceção de estímulos que possam comprometer a integridade dos seus tecidos possibilitando respostas de fuga ou de proteção. Esta competência é assegurada pelos mecanismos de nocicepção que são iniciados nas terminações periféricas dos nociceptores, fibras nervosas especializadas na transdução de estímulos químicos, físicos ou térmicos potencialmente nocivos. Os corpos celulares dos nociceptores que enervam a maior parte do corpo encontram-se reunidos ao longo da espinal medula nos gânglios da raiz dorsal (DRG, do inglês *Dorsal Root Ganglion*) enquanto que os das fibras que transduzem os estímulos nociceptivos da maioria dos tecidos craniofaciais têm os seus corpos celulares no gânglio trigeminal (TG, do inglês *Trigeminal Ganglion*). Devido ao seu elevado limiar de ativação, apenas estímulos de grande intensidade são capazes de ativar estes neurónios. Quando este limiar é atingido, a ativação de canais iónicos especializados leva à despolarização da membrana e à geração de um potencial de ação que é propagado ao longo do axónio do nociceptor até ao seu terminal central. Este faz sinapse com neurónios de segunda ordem na espinal medula que, por sua vez, transmitem a informação às estruturas cerebrais responsáveis pela integração da informação nociceptiva no contexto cognitivo e emocional, dando origem à experiência que conhecemos como "dor".

Apesar do seu importante papel fisiológico, em algumas situações, a dor deixa de ser um sinal de alarme para o potencial ou efetivo dano de tecidos, prolongando-se para lá do intervalo necessário para o processo de regeneração (geralmente é considerado um período de 3 meses). Nestes casos, a dor torna-se crónica e passa a ser ela própria uma patologia caracterizada pela presença de dor espontânea, hiperalgesia (os estímulos dolorosos passam a invocar uma sensação mais intensa), alodínia (estímulos que não eram dolorosos passam a sê-lo), parestesias (sensações anormais) e disestesias (sensações anormais e dolorosas). Quando a dor crónica afeta a região orofacial, o seu impacto torna-se ainda mais negativo devido à importância da cara e cabeça na formação da autoestima. São exemplo das síndromes que afetam esta região a enxaqueca, disfunções temporomandibulares, a neuralgia trigeminal e a dor facial idiopática. Para além dos episódios de dor que podem tornar-se muito frequentes ou mesmo constantes, as complicações associadas incluem anorexia, náuseas, fotofobia e fonofobia. Desta forma, não só o bem-estar físico fica comprometido como também o estado psicológico e vida social dos doentes são seriamente afetados. Em casos extremos estes transtornos estão também relacionados a um elevado risco de suicídio.

A dor crónica afeta 20% da população tendo grandes efeitos socioeconómicos. Contudo, ainda existe uma lacuna no que diz respeito ao conhecimento dos fenómenos patofisiológicos subjacentes, fator que resulta em tratamentos não são totalmente eficientes e ligados a efeitos secundários como a habituação e a dependência. Esta falha é ainda mais profunda no que diz respeito à dor orofacial uma vez que a maior parte dos modelos animais utilizados se concentra no estudo dos membros inferiores, devido à maior facilidade no que diz respeito ao acesso cirúrgico e aos procedimentos de teste comportamental.

Por trás da dor crónica estão mediadores químicos libertados pelos tecidos danificados e em situações de inflamação. Estas moléculas são responsáveis pela ativação de cascatas de transdução de sinal que culminam tanto em alterações funcionais rápidas como em alterações de longo termo ao nível da expressão genética. Uma das classes moleculares cuja expressão e função é afetada são os canais de potássio dependentes de voltagem (K_V). Estas proteínas membranares são ativadas por alterações no potencial de membrana e o fluxo de potássio por elas mediado é responsável pela repolarização da membrana durante os potenciais de ação. A família de canais K_V é extremamente diversa pelo que, além desta função, estes canais também estão envolvidos na regulação da excitação neuronal, do limiar de

ativação, da forma do potencial de ação, da frequência de disparo, entre outros. Desta forma, alterações nas propriedades biofísicas destes canais irão refletir-se no nível de excitabilidade neuronal.

O foco da presente dissertação são os nociceptores que enervam a região orofacial e as alterações sofridas pelos canais K_V num contexto de dor orofacial crónica. Para estudar estas modificações foi estabelecido um modelo animal através da injeção de uma emulsão de detritos bacterianos ativadora do sistema imunitário, o CFA (do inglês *Complete Freund'sAdjuvant*), na região perioral de ratos Wistar machos (N=3). Durante 28 dias o comportamento dos ratos foi monitorizado para avaliação da presença de alterações sensoriais. Os testes comportamentais incluíram a observação e quantificação de comportamentos espontâneos bem como a medição da sensibilidade mecânica da pele em redor das vibrissas. Embora a alterações observadas nos comportamentos espontâneos não tenham sido significativas, foi observada uma tendência que será explorada em trabalhos futuros. Não obstante, a existência de perturbações sensoriais foi confirmada pela redução do limiar de sensibilidade mecânica da zona mistacial.

Após 4 semanas, os animais foram sacrificados e os TG foram recolhidos para experiências de whole-cell voltage-clamp. Em condições controlo, as correntes registadas são caracterizadas por duas componentes: uma de inativação mais rápida (I_{Fast}) e outra de inativação mais lenta (I_{Slow}). A caracterização eletrofisiológica destas componentes em n = 34 neurónios de TGs provenientes de ratos naïve revelou a existência de duas populações que diferem nas expressões relativas de cada componente, uma descoberta que está de acordo com a literatura referente a TG e a DRG.

Geralmente as correntes de potássio são consideradas um "travão" da excitabilidade neuronal. No entanto, os resultados desta dissertação sugerem que numa situação de dor orofacial crónica estas correntes são potenciadas. Por um lado, a inativação da componente I_{Slow} está comprometida o que contribui para a potenciação da repolarização da membrana na fase final do potencial de ação, permitindo que um padrão de disparo frequente e repetitivo seja sustentável. Por outro lado, a componente I_{Fast} ativa-se a potenciais de membrana mais despolarizados, i.e., durante o potencial de ação a ativação destes canais ocorre mais tardiamente. Estes resultados, associados a uma inativação mais lenta da componente I_{Slow} indicam que os potenciais de ação propagados ao longo dos nociceptores são mais longos do que os da situação controlo, o que terá consequências ao nível da transmissão sináptica para o sistema nervoso central.

Tendo em conta resultados obtidos em experiências anteriores e o facto de as alterações observadas se concentrarem na componente lenta, foi também estudada a contribuição da subunidade $K_V1.3$ que se suspeita estar envolvida na patofisiologia da dor crónica (resultados não publicados) e medeia uma corrente cuja cinética está de acordo com os resultados obtidos.

Outro conjunto de resultados importantes está incluído na comparação entre as correntes observadas em neurónios do TG e neurónios dos DRG. Não só não foram detetadas diferenças significativas ao nível das correntes controlo, mas também as alterações observadas no contexto de dor orofacial crónica são concordantes com os resultados obtidos em modelos de dor nas patas traseiras. Deste modo, pode admitir-se que a dor orofacial crónica partilha alguns mecanismos com a dor crónica noutras regiões corporais o que poderá ser explorado no desenvolvimento de futuros fármacos.

Deste modo, no presente trabalho estabeleceu-se que 1) a injeção de CFA na região perioral dá origem a perturbações sensoriais de longa duração (28 dias); 2) no contexto de dor orofacial crónica as correntes de potássio sofrem modificações que permitem uma situação de atividade neuronal exacerbada mantendo a homeostasia, podendo também estar envolvidas em mecanismos de sensibilização do sistema nervoso central e 3) é possível que alguns mecanismos envolvidos no estabelecimento da dor orofacial crónica estejam também implicados no desenvolvimento da dor crónica noutras regiões corporais, representado possíveis alvos terapêuticos.

Palavras-chave: Dor crónica; dor orofacial; canais de potássio dependentes de voltagem; gânglio trigeminal.

ABSTRACT

The perception of noxious environmental stimuli is essential for protection and survival. Along with cognitive and emotional brain processing, the nociceptive input gives rise to the complex experience known as "pain". The noxious mechanical, chemical, and thermic stimuli are transduced by specialised neurones, the nociceptors, whose cell bodies are found in the dorsal root ganglia (DRG) and the trigeminal ganglion (TG). These afferent fibres synapse to second-order neurones in the dorsal horn of the spinal cord, which in turn project to the higher centres responsible for eliciting the consciousness of pain.

When pain persists for longer than 3 months, the period considered necessary for tissue regeneration, it becomes chronic and no longer serves its biological purpose. This condition is characterised by spontaneous pain, hyperalgesia (painful stimuli evoke a more intense response), allodynia (innocuous stimuli become painful), paraesthesias (abnormal sensations), and dysesthesias (painful paraesthesias). The orofacial region is the site of several chronic pain syndromes such as migraine, temporomandibular disorders, trigeminal neuralgia, and persistent idiopathic facial pain. Associated with these disorders, there is a loss of quality of life that often manifests in depression. Due to the lack of knowledge about the mechanisms underlying these conditions, the available treatments are not effective and are associated with unpleasant side effects such as habituation and addiction.

Chronic pain conditions are characterized by an augmented neuronal excitability induced by mediators released during injury and inflammatory conditions. Central to the setting of neuronal excitability is the voltage-gated potassium (K_V) channel family. These membrane proteins are responsible for the regulation of resting membrane potential, action potential threshold, shape, firing frequency, and adaption.

The focus of the present dissertation was the K_V-mediated currents of small-diameter neurons from the TG, where the cell bodies of the fibres innervating the craniofacial region are found. These currents were characterised both in naïve and chronic pain conditions. Additionally, the currents obtained from TG neurons of naïve animals were compared with the currents from DRG neurons, the "spinal analogue" of the TG.

An animal model for chronic inflammatory orofacial pain was established through subcutaneous administration of complete Freund's adjuvant (CFA) to the whisker pad of male Wistar rats (N=3). The degree of nociceptive disturbance was evaluated both by changes in the spontaneous behavioural activity and the withdrawal threshold upon mechanical stimulation. The results show that following CFA injection, the animals displayed signs of altered nociception and increased sensibility lasting up to 28 days. Despite the lack of significant differences in spontaneous behaviours, suggestive tendencies were observed.

After the 4 weeks period, the rats were euthanised and the TG neurons were dissociated and used for whole-cell voltage-clamp recordings. The electrophysiological results suggest that in a chronic pain condition the K_V currents (traditionally viewed as a neuroexcitability "brake") are surprisingly intensified. The inactivation of the slower current component is compromised and its kinetics is even slower in the chronic pain model. Moreover, the fast current component is activated at more depolarized membrane potentials. Thus, it can be concluded that in the context of chronic orofacial pain K_V currents are modified allowing for an exacerbated neuronal activity while maintaining a homeostatic mechanism

Furthermore, the altered K_V currents may be involved in the long-term sensitization of the central nervous system.

The results also suggest the existence of shared mechanisms between orofacial chronic pain and chronic pain in other body regions since no significant differences were found in the biophysics of K_V currents of both TG and DRG neurones. Additionally, the changes observed in this chronic pain model

are consistent with previous findings in models focused in the hind paw. Furthermore, the presence and function of $K_V1.3$, a channel subunit formerly implicated in the pathophysiology of chronic pain (unpublished results), was confirmed.

In conclusion, the present dissertation suggests new mechanisms underlying chronic orofacial pain hinting at possible new therapeutic approaches.

Keywords: Chronic pain; orofacial pain; voltage-gated potassium channels; trigeminal ganglion

TABLE OF CONTENTS

Acknowledgements II
Resumo III
Abstract VI
Table of Contents VIII
Tables and Figures X
Abbreviations XI
1 Introduction 1
1.1 From Nociception to Pain 1
1.2 From Physiological to Chronic Pain 2
1.3 The Trigeminal Sensory System 3
1.4 Orofacial Chronic Pain 4
1.5 Animal Pain Models 5
1.5.1 Orofacial Pain Models 5
1.5.2 The Assessment of Orofacial Pain 6
1.5.2.1 Spontaneous Behaviour 6
1.5.2.2 Elicited Responses 6
1.6 Voltage-Gated Potassium Channels 7
1.6.1 Role in neuroexcitability 8
2 Goals 9
3 Methods 9
3.1 Animals 9
3.2 Behavioural Testing 9
3.2.1 Non-Evoked Behaviour 9
3.2.2 Mechanical Sensitivity 10
3.3 Chronic Inflammation Induction 10
3.4 Acute Cell Dissociation 10
3.4.1 Trigeminal Ganglia 10
3.4.2 Dorsal Root Ganglia 11
3.5 Whole-cell Voltage Clamp 11
3.5.1 Data Analysis 11
3.6 Pharmacological Experiments 12
3.7 Statistical Analysis 12
4 Results 13
4.1 Behavioural Testing 13

4.1.1 Spontaneous Behaviour 13
4.1.2 Mechanical Sensitivity 14
4.2 Electrophysiology 14
4.2.1 K^+ Currents in Small-Diameter Trigeminal Ganglion Neurones 14
4.2.1.1 Voltage-Dependence of Activation 15
4.2.1.2 Voltage-Dependence of Inactivation 16
4.2.2 K+ Currents in a Model of Chronic Orofacial Pain 17
4.2.2.1 Voltage-Dependence of Activation 17
4.2.2.2 Voltage-Dependence of Inactivation 19
4.2.3 K^+ Currents in Small-Diameter Sensory Neurones 21
4.2.3.1 Voltage-Dependence of Activation 21
4.2.3.2 Voltage-Dependence of Inactivation 23
4.3 Pharmacological Experiments 24
5 Discussion 24
5.1 CFA-Induced Chronic Inflammatory Hyperalgesia 24
5.1.1 Spontaneous Behaviour 25
5.1.2 Mechanical Sensitivity 25
5.2 Inflammation-induced changes in K^+ currents 25
5.3 $K_V1.3$: a Potential Target 26
6 Conclusions 27
6.1 Future Directions 27
7 References 28

TABLES AND FIGURES

Table 1.1 Orofacial Pain Models. 5
Table 4.1 Double Boltzmann fitting parameters for the inactivation profile of both components. 21
Table 4.2 Boltzmann fitting parameters of the activation curves. 22
Table 4.3 Double Boltzmann fitting parameters for the inactivation profile of small-diameter sensory neurones. 24

Figure 1.1 Nociceptive fibre classification. 1
Figure 1.2 Schematic representation of the pain pathway. 2
Figure 1.3 Diagram of the sensitization process. 3
Figure 1.4 Schematic representation of the trigeminal sensory system. 3
Figure 1.5 Orofacial Chronic Pain Classification according to Woda and colleagues [20]. 4
Figure 1.6 Schematic representation of the rodent trigeminal system. 6
Figure 1.7 Potassium channels classes and gating mechanisms. 7
Figure 1.8 K_V channel structure. 8
Figure 4.1 Mean episode duration of the studied non-evoked behaviours. 13
Figure 4.2 Withdrawal Threshold. 14
Figure 4.3 Whole-cell K^+ current in a small-diameter TG neuron. 15
Figure 4.4 Typical K^+ current traces of two major types of voltage clamp recordings observed in small-diameter TG neurones. 15
Figure 4.5 Activation profile of K^+ currents in small-diameter TG neurones. 16
Figure 4.6 Voltage dependence of activation and Voltage dependence of kinetics. 16
Figure 4.7 Voltage dependence of inactivation 17
Figure 4.8 Changes in the activation profile. 17
Figure 4.9 Changes in current density. 18
Figure 4.10 Changes in the voltage dependence of kinetics. 19
Figure 4.11 Changes in the voltage dependence of activation. 19
Figure 4.12 Changes in the inactivation profile. 20
Figure 4.13 Changes in the voltage dependence of inactivation. 20
Figure 4.14. Activation profile of K^+ currents in small-diameter sensory neurones. 21
Figure 4.15 Current density of K^+ currents in small-diameter sensory neurones from TG (black) and DRG (green). 22
Figure 4.16 Voltage dependence of activation of K^+ currents in small-diameter sensory neurones from TG (black) and DRG (green). 22
Figure 4.17 Inactivation profile of K^+ currents in small-diameter sensory neurones. 23
Figure 4.18 Voltage dependence of inactivation of K^+ currents in small-diameter sensory neurones from TG (black) and DRG (green). 23
Figure 4.19 Effect of PAP-1 (2nM) on small-diameter TG neurones. 24

ABBREVIATIONS

AF	Asymmetric Facial-Grooming
AP	Action Potential
B	Body-Grooming
BF	Facial-Grooming during Body-Grooming
C	Capacitance
CCI	Chronic Constriction Injury
CFA	Complete Freund Adjuvant
DRG	Dorsal Root Ganglia
E	Exploratory Behaviour
F	Freezing-like behaviour
FG	Facial-Grooming
G	Conductance
I	Current
I_A	A-current
IAN	Inferior Alveolar Nerve
IASP	International Association for the Study of Pain
I_D	D-current
I_K	K-current
I_M	M-current
I_{Na}	Sodium Current
ION	Infraorbital Nerve
J	Current Density
K^+	Potassium Ion
K_V	Voltage-gated Potassium Channel
Na^+	Sodium Ion
Na_V	Voltage-gated Sodium Channel
PD	Pore Domain
SF	Spontaneous Facial-Grooming
TG	Trigeminal Ganglia
TMJ	Temporomandibular Joint
TN	Trigeminal Neuralgia
$V_{1/2}$	Voltage of half activation or inactivation
Vm	Membrane potential
V_S	Slope factor
VSD	Voltage-Sensing Domain
τ	Time-constant

1 INTRODUCTION

1.1 FROM NOCICEPTION TO PAIN

Pain is a complex experience involving the transduction of noxious environmental stimuli along with cognitive and emotional processing by the brain [1]. This sensory mechanism starts skin-deep with specialised neurones, the nociceptors, that recognise potentially tissue-damaging stimuli. The resulting signals are conveyed to the central nervous system eliciting escaping behaviours that are critical to survival. Nociceptors differ from primary sensory neurones of other sensory systems because they are completely autonomous from any kind of specialised receptor cells, i.e. the cell responsible for stimulus detection is the same one that conducts the information [2]. Nociceptive fibres also have a particularly high variety of transduction mechanisms allowing them to sense a more diversified scope of stimulus modalities [3].

Mammalian nociceptors have been classified according to conduction velocity, diameter, amount of myelination, and types of stimuli to which they respond (Figure 1.1). This heterogeneity relates to specific functions and detection of several pain modalities [4]. There are two broad classes of nociceptive fibres: Aδ-fibers and C-fibers. While the first group consists of medium-diameter thinly myelinated fibres that transduce acute, well-localized pain, C-fibers are small-diameter unmyelinated fibres that transduce delayed, diffuse pain [4,5]. Since the intensity of potentially damaging stimuli differs according to the tissue considered, nociceptors from different tissues have distinct features resulting in different mechanical thresholds and overall sensitivity [3,6].

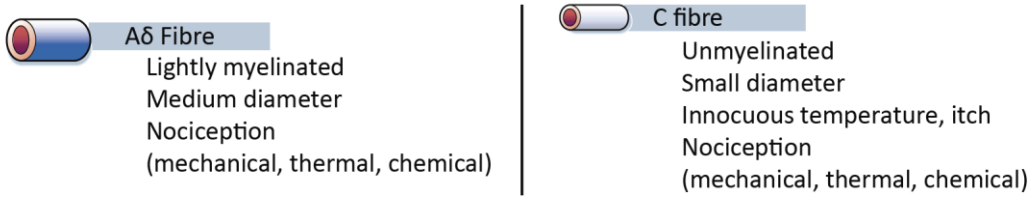

Figure 1.1 **Nociceptive fibre classification**.
Each type of nociceptor is responsible for the transduction of a different type of pain: medium-diameter myelinated fibres (Aδ) detect acute well-localized pain while small-diameter unmyelinated fibres (C) relay delayed, poorly localised pain. Adapted from [3].

The peripheral terminals of the nociceptors transduce external stimuli into electrical signals, generating action potentials (APs) when the activation threshold is reached [7]. Through mechanisms later discussed, the APs are propagated along the axons of these cells whose cell bodies are found in the peripheral nervous system, in the dorsal root (DRG) and the trigeminal (TG) ganglia [4]. From the peripheral ganglia, the nociceptive sensory signals are transmitted to neuronal circuits in the dorsal horn of the spinal cord [8,9]. These second-order neurones project to the brain stem or to the thalamocortical system, inciting the conscious pain response [4] mediated by neural networks responsible for the sensory-discriminative and affective components of the pain response (Figure 1.2) [6]. Therefore, while nociception is the perception of stimuli that threaten tissue integrity, pain itself only occurs after the brain processes the resulting signals culminating in an "unpleasant sensory and emotional experience", as described by the International Association for the Study of Pain (IASP). Since nociception and pain are independent mechanisms, one can take place in the absence of the other [7]. In such scenarios, pain becomes dysfunctional and pathological as it will be discussed subsequently.

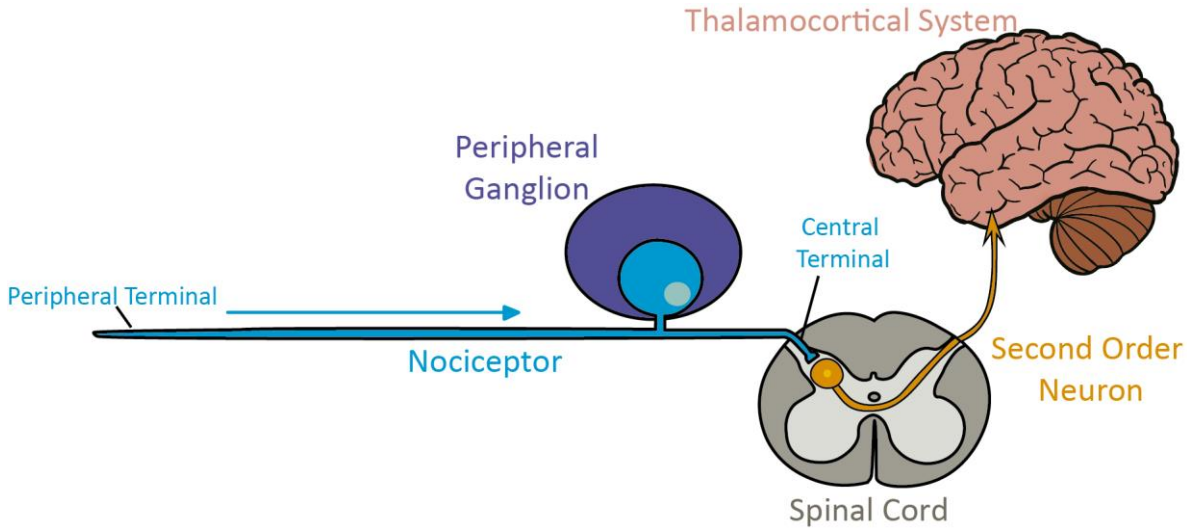

Figure 1.2 **Schematic representation of the pain pathway.**
The peripheral terminal of nociceptors detects external stimuli and produce electrical signals that are conveyed to second order neurones in the spinal cord. These fibres make up an ascending pathway to the thalamocortical system responsible for the conscious pain response.

1.2 FROM PHYSIOLOGICAL TO CHRONIC PAIN

Acute or physiological pain is a normal response to noxious stimuli and has a protective role against actual or potential damage by eliciting withdrawal reflexes. However, inflamed or injured tissue may display seemingly spontaneous pain, hyperalgesia (abnormal pain response caused by a noxious stimulus), allodynia (pain induced by normally innocuous stimulation), paraesthesia (abnormal sensation), and dysesthesia (abnormal and uncomfortable sensation) which are symptoms of pathological pain [6,8].

Pathological pain is a result of plastic changes that take place along the pain transduction pathways. The plasticity of the somatosensory system is responsible for changes both in the peripheral afferents that are stimulated by the original injury (peripheral sensitization) and in the spinal cord neurones (central sensitization) (Figure 1.3) [3,10,11]. Behind these changes is the action of mediators released by cells affected by injury or inflammation. Such molecules modulate the activity of receptors and ion channels through, not only rapid functional changes but also long-term alterations in the gene expression [6,12].

The activity of the inflammatory mediators culminates in an altered neuronal basal sensitivity, increasing the responsiveness of nociceptors whose persistent hyperexcitability may lead to further changes in the sensory pathways [6,13]. In the central nervous system, changes in gene expression such as upregulation of central acting neuromodulators and respective receptors generate an augmented pain response [13]. Furthermore, even the neuronal phenotype can also be modified as A-fibers may acquire neurochemical features typical of C-fibers contributing to stimulus-induced hypersensitivity [10].

Both peripheral and central sensitization lead to pain persistence and, according to the IASP, pain becomes chronic when it lingers for longer than 3 months, the normal time required for tissue healing. At this point, pain no longer serves its biological purpose as a symptom of damage and becomes a pathology itself, i.e. becomes chronic [14].

Roughly 37% of the Portuguese and 20% of the European adult population suffers from chronic pain [15,16]. The persistent (and sometimes constant) discomfort has a negative effect on life quality. Additionally, to the personal burden, the estimated financial cost of chronic pain amounts to €200 billion per annum in Europe [16]. Despite the recent advances in the understanding of the mechanisms behind chronic pain, the management of this health issue is still unsatisfactory for two-thirds of sufferers [16].

These numbers show that further investigation should be carried out in order to identify novel therapeutic targets and approaches.

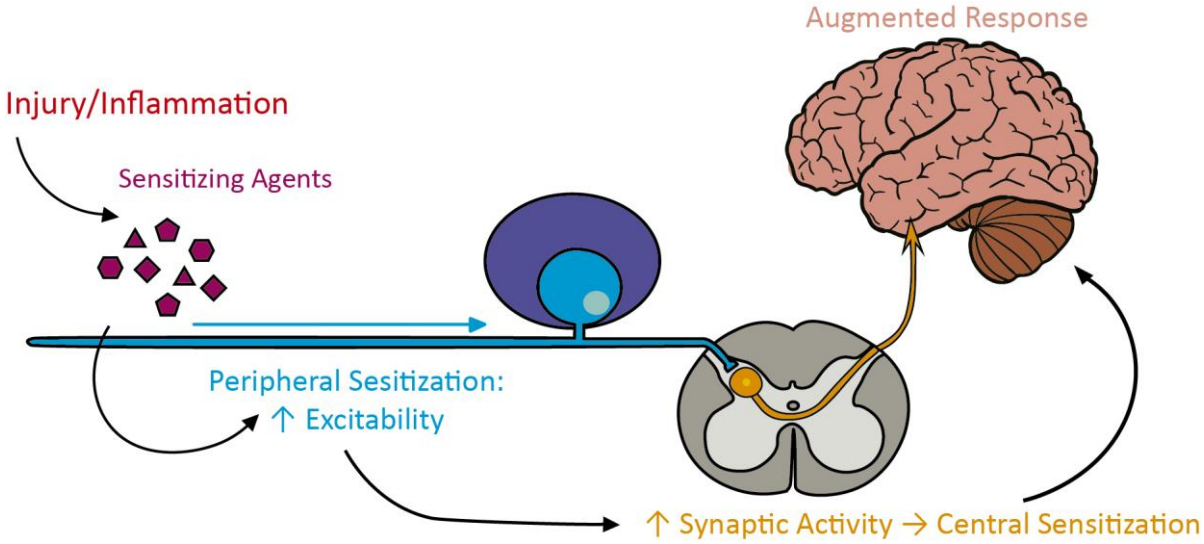

Figure 1.3 **Diagram of the sensitization process.**
The presence of sensitizing agents resulting from injury or inflammation leads to changes in the excitability of the pain pathway leading to an augmented response.

1.3 THE TRIGEMINAL SENSORY SYSTEM

The trigeminal nerve is responsible for the innervation of most craniofacial tissues (Figure 1.4). By eliciting withdrawal reflexes this nerve contributes to the maintenance of the tissue integrity. This function is of paramount importance as most sensory and homeostatic systems are located in the head. Compared to the spinal systems, at the functional level, the trigeminal sensory system is more complex. This complexity is due to some unique characteristics such as the embryological origin, the proportion of myelinated, unmyelinated and sympathetic fibres, and the location of some branches within bony canals [9,17].

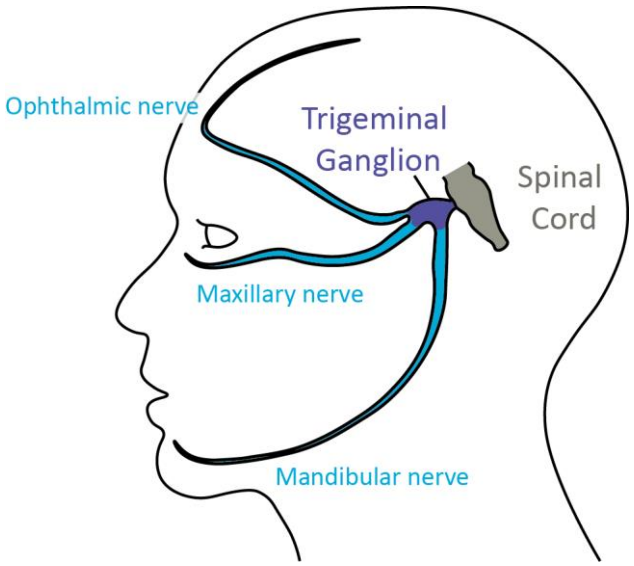

Figure 1.4 **Schematic representation of the trigeminal sensory system.**
The trigeminal ganglion aggregates the cell bodies of the three branches of the trigeminal nerve: the ophthalmic nerve, the maxillary nerve, and the mandibular nerve. The central projections of these fibres synapse with second-order neurones of the trigeminal spinal nucleus on the spinal cord.

Contrary to what happens in other main nerve trunks, most of the trigeminal nerve is purely sensory, as its fibres are sensitive to mechanical, thermal, and chemical stimuli. The small motor component of the mandibular branch is clearly detached and the cell bodies of these fibres are located in the mesencephalic trigeminal nucleus, the only known nucleus situated within the central nervous system containing the cell bodies of primary afferent neurones [18,19].

1.4 OROFACIAL CHRONIC PAIN

Orofacial pain syndromes incorporate a wide spectrum of conditions ranging from acute and transient conditions such as most toothaches and headaches to chronic conditions that may persist for several years [20]. Complications often linked with these disorders include anorexia, nausea, vomiting, photophobia, and phonophobia. Besides, the severe chronic pain and the emotional meaning of the craniofacial region add to the psychological burden that often manifests in depression and, less frequently, an increased suicide risk among sufferers [14,21].

Since most of the basic science research into the pain mechanisms has been done in the limbs and trunk, the aetiology and pathogenesis of most trigeminal nerve-related chronic pain conditions are still unknown which is the reason behind a poor diagnosis and management [18,20,21]. Most diagnostic and classification criteria are based on individual expert opinion and, thus, not objective nor standardized. These classification systems are particularly problematic considering that the same condition may have different clinical manifestations, presenting itself as distinct symptom combinations that lead to inconsistent classification and diagnosis [20].

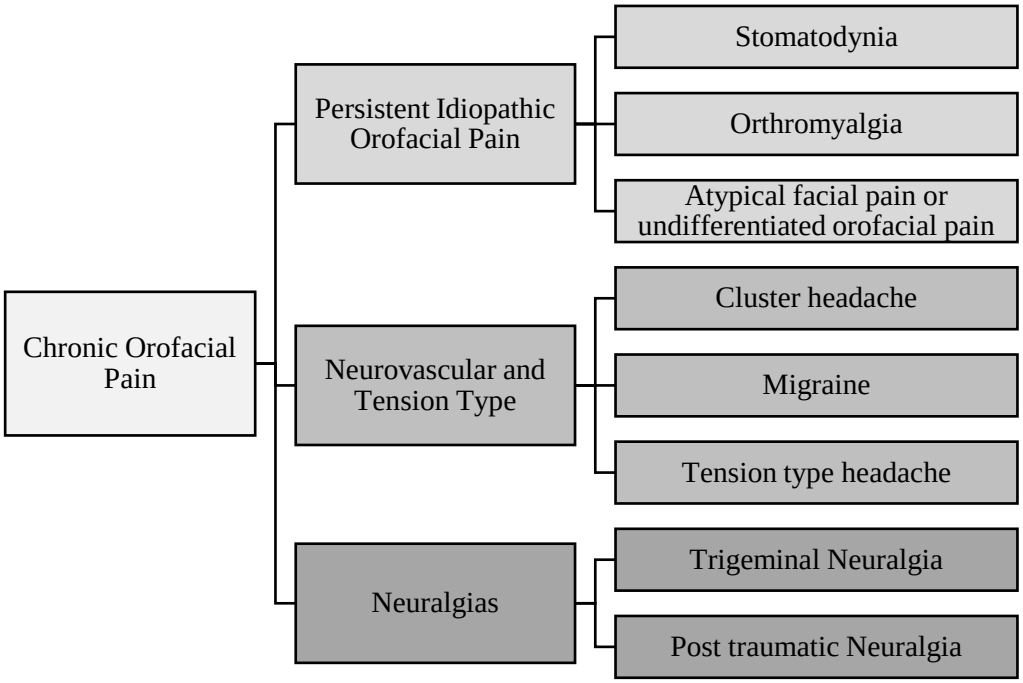

Figure 1.5 **Orofacial Chronic Pain Classification according to Woda and colleagues [20].**
This classification was developed as an effort to avert current methods that are susceptible to topographical characteristics, giving rise to unnecessarily complex classifications [20].

Woda and colleagues proposed a classification of orofacial chronic pain conditions, dividing them into persistent idiopathic orofacial pain, neurovascular and tension-type, and neuralgias (Figure 1.5) [20]. The "orofacial neuralgias" are mainly neuropathic conditions. In fact, trigeminal neuralgia (TN) is considered the prototype of neuropathic pain in the trigeminal region. Curiously, however, the system used for the diagnosis of neuropathic pain does not apply to classical TN [22]. On the other hand, most persistent idiopathic orofacial pain disorders have an inflammatory component [14,23,24]

1.5 ANIMAL PAIN MODELS

Animal models are the core of the pain research and drug development effort as the study of the pain mechanisms can be done in a standard genetic and environmental background. Even though the sensitization mechanisms are similar to the ones observed in humans, as pain is a very subjective experience, all the sensory, emotional, and cognitive components are not always easily incorporated in animal models [25,26]. Notwithstanding, meticulous behavioural analysis methods have been developed in order to quantify pain as objectively as possible [27,28].

1.5.1 Orofacial Pain Models

Bennet and Xie [29] developed perhaps the most extensively used animal pain model: the chronic constriction injury (CCI) to the sciatic nerve. This is such a well-established model that one of the first efforts to study chronic orofacial pain was its adaptation to the infraorbital nerve (ION) by Vos and colleagues [28]. Since then, both the CCI model and several other injury modalities have been employed in several portions of the trigeminal nerve (Table 1.1). Generally, these models induce an hyperexcitable state that reflects in the function and expression of several molecules as well as the neuronal electrophysiological properties.

As far as the inflammatory orofacial pain models are concerned, fewer variations have been made through the years. Inflammation is usually induced by injecting an inflammatory agent such as Complete Freund's Adjuvant (CFA) or carrageenan, into an area enervated by the trigeminal nerve, most commonly the temporomandibular joint (TMJ). The peripheral inflammation triggers nociceptive sensitivity through the action of proinflammatory mediators that not only directly activate the nociceptors but also modulate the activity of receptors and ion channels [12,30]. The resultant inflammatory response may even cause mild nerve damage, magnifying its impact on neuronal excitability.

Despite the significant clinical interest, the number of studies in the orofacial region is disproportionally low compared to other body regions, namely the hind paws [18]. Such contrast may be a result of the combination of complex neuroanatomy, difficult model induction (especially when surgery is involved), and laborious behavioural testing.

Table 1.1 **Orofacial Pain Models.**
Orofacial pain models are often adaptations of models established for other body regions. Figure 1.6 represents the rodent trigeminal system for a clearer interpretation. For a more extensive review see [18].

	Model	References
Neuropathic pain models	Compression of the TG	31,32
	Chronic Constriction Injury of the Infraorbital Nerve (CCI-ION)	28,33–38
	Infraorbital Nerve Constriction	39
	Spared Nerve Injury applied to the ION	40
	Partial ION Ligation	41
	Unilateral CCI of the distal ION	38
	ION Axotomy	37
	Inferior alveolar nerve (IAN) Transection	42–46
	Photochemical injury to the IAN	47
	Tight Ligation of the mental nerve	48
Inflammatory pain models	Temporomandibular Joint Inflammation (TMJ-CFA)	49–51
	Whisker Pad/Perioral Inflammation	23,52,53
	Application of CFA to the orbital portion of the ION	54

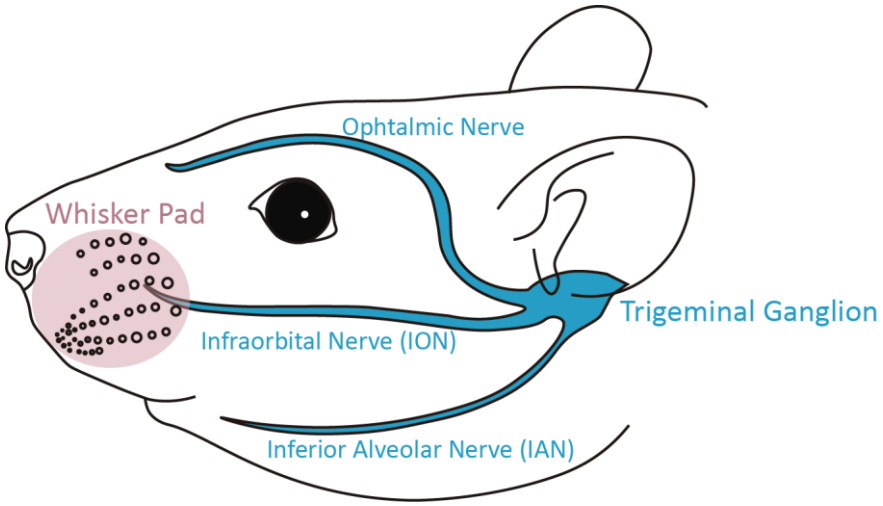

Figure 1.6 **Schematic representation of the rodent trigeminal system.**
Among the main trigeminal nerve branches, the infraorbital nerve (ION) is by far the most studied. This branch innervates the whisker pad, a very sensitive region that is crucial for the interaction between the animal and its environment.

1.5.2 The Assessment of Orofacial Pain

Due to the complexity and subjectivity of the pain experience, its assessment is a challenging task, especially in non-human animals that cannot self-report. In this case, behavioural cues and general behavioural changes are objectively scored and used as an indication of sensory disturbance [18,55]. Generally, two behaviour types can be evaluated: spontaneous behaviour and elicited responses [18].

1.5.2.1 Spontaneous Behaviour

Changes in non-evoked behaviour are considered a sign of spontaneous pain, a very relevant aspect of animal pain models due to the high prevalence of either continuous or paroxysmal pain attacks amongst chronic pain patients. Unfortunately, since rodents tend not to display visible signs of pain, the affected behaviour is hard to detect and describe. Vos and colleagues have comprehensively studied rat behaviour following ION-CCI, defining a behavioural categorization that has been widely adapted and used in orofacial pain research [28]. However, the low frequency and high variability of such behaviours are obstacles to their applicability: most of the times the observable changes are too subtle to quantify [18]. In addition, it remains unclear whether these behaviours are indicative of actual pain or another type of sensory disturbance [27,55].

Asymmetric facial-grooming is the most used behavioural indication of orofacial pain. When not related to pain, grooming appears to be a series of highly organised actions. On the other hand, moderate to intense irritation tends to elicit asymmetric grooming episodes directed to the stimulated area [27,28]. Furthermore, hair loss and superficial injury to the vibrissal pad, signs of excessive facial-grooming resulting from a persistent sensory disturbance, are sometimes observed in pain studies [47].

1.5.2.2 Elicited Responses

Study stimulus-evoked behaviour in the orofacial region is a challenging endeavour [18]. This area has a very rich mechanosensory receptor sheet and is stimulated almost continuously during exploratory behaviour. The active movement of the head and complex whisker activity are additional hurdles. In this aspect, it is essential to carry out habituation to testing procedures before any measurements, in order to reduce stress and reflex responses elicited by the approaching of the testing devices.

There are many arguments against using elicited responses as a measurement of pain and many questions arise from the fact that withdrawal responses evaluated assess nociception rather than actual pain [55]. They are also measures of hypersensitivity which is not as prevalent as spontaneous pain in the

clinical manifestations of chronic pain. Nonetheless, given how problematic it is to measure spontaneous pain, these seem to be the most objective and reliable pain assessment methods [56].

For a correct stimulus application, restraint is also often required, introducing an additional stress-inducing factor. Several methods are used, from holding the animal by the experimenter [47,48,50] to testing unrestraint animals [28,35,38,41].

1.6 VOLTAGE-GATED POTASSIUM CHANNELS

During the sensitization process studied with the aforementioned models, many molecular classes are modulated leading to an increase of the excitability of the afferent fibres. The ion channels are one of the classes involved in setting the neuronal excitability levels and therefore their expression and function are altered in pain models. Here is presented a brief review of the function and structure of voltage-gated potassium (K_V) channels.

Due to their impermeability to ions, cell membranes generate an electrochemical gradient across their surface. However, these bilipidic barriers have breaches: ion channels, integral membrane proteins whose hollow centres selectively conduct ions. A crucial characteristic of ion channels is their ability to respond to gating signals, opening and closing only when appropriate allowing some control of the intracellular ionic composition [57,58].

Potassium (K^+) channels are one of the most diverse and ubiquitous families of membrane proteins [59]. Most cells express various K^+ channels subtypes that have several gating mechanisms and functional properties (Figure 1.7) and are critical for many physiological processes [60,61].

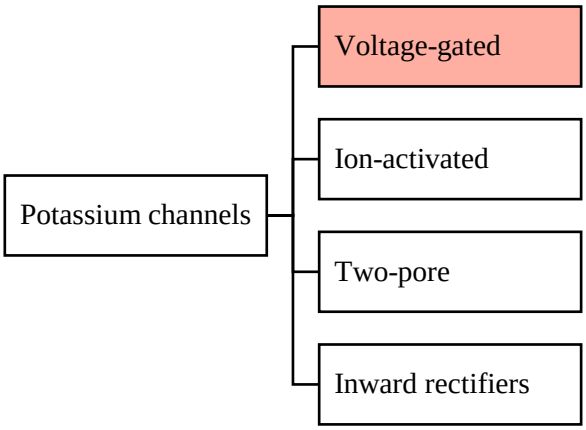

Figure 1.7 **Potassium channels classes and gating mechanisms**.
The focus of this thesis will be voltage-gated (K_V) channels that activate in response to changes in membrane potential. Ion-activated potassium channels include calcium-activated channels that respond to changes in intracellular ionic concentration, two-pore K^+ channels mediate "leak" currents, and inward rectifier K^+ channels conduct atypical inward currents [59].

By responding to changes in membrane potential (Vm), K_V channels have an essential role in various cellular processes [60]. A functional K_V channel is formed by a tetramer of α-subunits each consisting of six transmembrane domains (S1-S6) (Figure 1.8). Each α-subunit has two structural and functional different sections. While the helices S1-S4 make up the voltage-sensing domain (VSD) and are responsible for the detection of changes in the Vm, the S5 and S6 domains constitute the central pore (PD) that conducts K^+ ions and includes two components: a selective filter and a channel gate. [60]. The main function of the filter is to only allow K^+ ions to flow. This is achieved due to the interaction of the carbonyl groups of this segment with the K^+ ions. By substituting the hydration waters, the carbonyl groups help overcome the disadvantageous electrostatic forces, making the entry of ions into the membrane energetically favourable [58]. Apart from the extracellular (upper) gate formed by the conserved P-region of the selectivity filter, K_V channels also have an intracellular gate formed by the S6 of the four

α-subunits that is controlled by external stimuli such as the Vm [60] Additionally, many K^+ channels are also associated with auxiliary proteins or β-subunits that can modulate channel properties.

Functionally K_V channels have three states: closed, activated, and inactivated. The exact mechanism by which these channels activate is subject of ongoing debate [60] but it is believed that when the membrane depolarises the positively charged S4 domain rearranges itself across the membrane creating a pathway for ionic flux [62]. If the membrane depolarization is maintained, most K_V channels inactivate. So far two mechanisms of inactivation have been described. The N-type inactivation is a faster process involving an inactivation peptide that enters the pore preventing the passage of ions. On the other hand, the slower C-type inactivation is mediated by the selectivity filter that closes blocking ion flow. When the Vm returns to the resting level, the channels return to their closed conformation [60].

In the context of chronic pain and the associated increase in the neuronal excitability, all the functional states that can be adopted by the K_V channels are liable to modulations that are reflected on the biophysical properties of the channel.

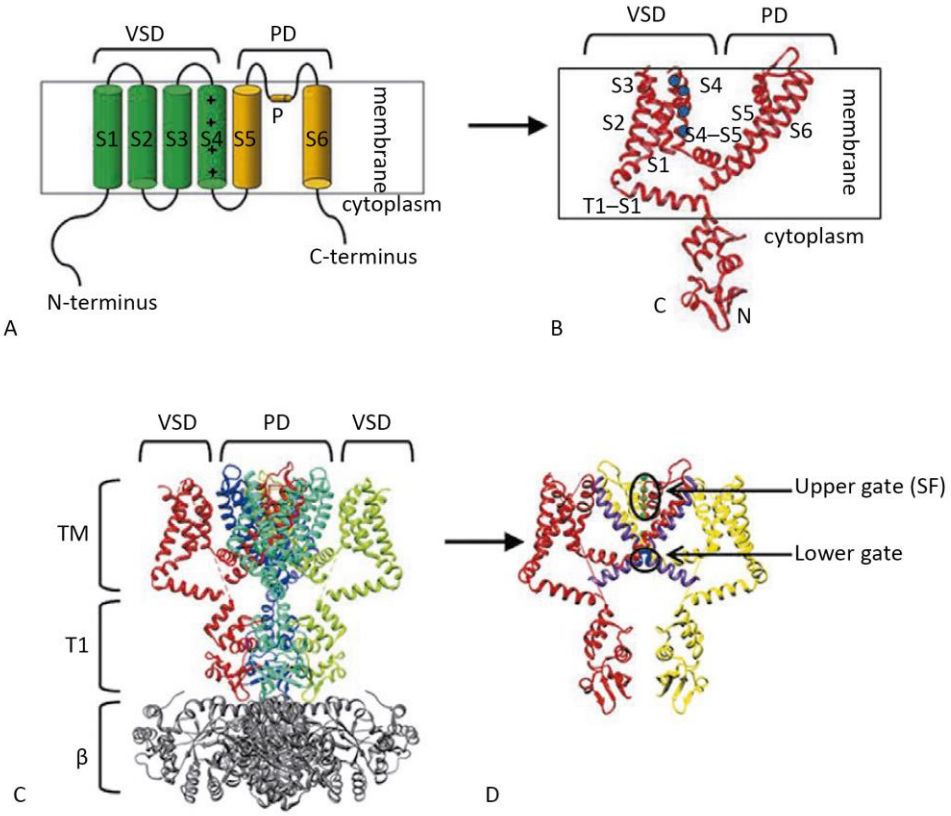

Figure 1.8 **K_V channel structure.**
A – Diagram of a single α-subunit. The positive charges of the S4 segment are represented. B – Crystal structure of an α-subunit of the $K_V1.2$ channel. C – Crystal structure of the $K_V1.2$ channel in a complex with a β-subunit. D – Gating of the $K_V1.2$ channel. Only two opposite α-subunits are represented. Reproduced from [60]

K^+ currents can be distinguished based on their kinetics: K-current (I_K) is a sustained current that inactivates slowly, A-current (I_A) inactivates rapidly and is transient, D-current (I_D) consists on a transient current that inactivates slowly, and M-current (I_M) is one that does not inactivate. Each of these currents is mediated by different types of channels and depending on channel expression and function the dynamic of the K^+ currents at the cellular level may be modified [63].

1.6.1 Role in neuroexcitability

After a depolarising event, voltage-gated sodium (Na_V) channels are recruited. As sodium enters the cell, the membrane potential rises and, if the firing threshold is reached, an AP is generated. The

potential reached leads to the opening of high-threshold K_V channels that mediate an outward movement of K^+ ions contributing to the membrane repolarization [57,64]. Nevertheless, sensory neurones express an array of functional types of K_V channels with distinct kinetic responses. Therefore, additionally to repolarization of APs, K^+ channels have a major role in the regulation of membrane potential, action potential shape, firing adaptation and overall cellular excitability [61]. For instance, some K^+ channels conduct a persistent background current that opposes the depolarising influences of Na_V channels at subthreshold potentials [57,64].

The particular channel expression pattern in each neuron may be adapted according to excitability requirements [65]. An example is the changes reported in orofacial pain models. These studies report a general decrease on K^+ currents, namely I_K and I_A [33,42,43,49]. On the other hand, the potassium current activated by hyperpolarization is augmented [33]. However, none of these models studied the effects of chronic pain in small-diameter TG neurones.

2 GOALS

The present work aims to characterize the K_V current components from small-diameter TG neurones, not only in naïve animals, comparing them to DRG neurones, but also in a context of chronic pain. In order to achieve this main objective, several goals were defined:

- Establish a chronic inflammatory orofacial pain model and validate it through behavioural analysis and quantification of mechanical hyperalgesia;
- Characterize of the K_V current components of small-diameter TG neurones obtained from both naïve and chronic pain conditions through whole-cell voltage-clamp;
- Compare the obtained results to the ones inferred from small-diameter DRG neurones in order to investigate possible shared and/or specific mechanisms underlying the painful sensations of different anatomical areas.

3 METHODS

3.1 ANIMALS

Male Wistar rats were purchased from NMS|FCM and maintained in a 12 : 12 h light : dark cycle (lights on at 07.00 h) at 21 ± 3 º C, fed *ad libitum*. Animal care and experimental studies were in accordance with Directive 2013/63/EU

3.2 BEHAVIOURAL TESTING

Behavioural testing was performed in a lowly lit room, always at the same time of the day and by the same experimenter. Rats were habituated to the room, the experimenter, and the testing procedures for a week before the model was induced. The measurements obtained in the last three days of habituation were used to establish a baseline level of responsiveness. Following CFA-induced inflammation, behavioural testing was performed at days 3, 7, 14, 21, and 28 post-injection.

3.2.1 Non-Evoked Behaviour

To evaluate changes in general behaviour activity, rats were placed in a transparent acrylic cage and the observed behaviour was classified as (E) exploratory behaviour such as walking, running, climbing, rearing, and sniffing; (F) freezing-like behaviour during which the animal adopted an

immobile posture; (B) body-grooming during which the paws, tongue, or incisors contacted with a body part other than the face or the forepaws; or (FG) face-grooming the paws contacted facial areas. Finally, face-grooming activities were classified based on the context in which they were performed: (SF) spontaneous face-grooming that was neither preceded nor followed by body grooming; (BF) face-grooming during body-grooming if body-grooming occurred before or after a sequence of face-grooming actions; and (AF) asymmetric face-grooming when the face-grooming actions were directed only to one side of the face [28]. The number and duration of episodes were determined for each 7-min observation period.

To minimise the natural inter-individual variability, the mean values of the last three days of the habituation period were used as a baseline to which all values were normalised.

3.2.2 Mechanical Sensitivity

To measure the mechanical withdrawal threshold, the animals were gently restrained with a towel, allowing movements of the head and front paws, and von Frey filaments of increasing force were applied within the infraorbital nerve territory, on the hairy skin surrounding the mystacial vibrissae, at a 90º angle until bent. Each filament was tested 5 times on each side with at least 5 seconds interval between stimuli making sure that the same site was not repeatedly stimulated. Response scoring was based on Vos et al. 1994: positive responses include withdrawal reaction during which the rat turned the head away when stimulated, sometimes accompanied with a single face swipe which was scored as 1; escape/attack response was scored as 2 and was defined as active avoidance of further contact with the stimulus object and/or making biting and grabbing actions towards it; the maximal score of 3 was used for asymmetric face-grooming responses. When the animal turned the head to the stimulating object and explored it, sniffing or licking it, the response was considered as simple detection and was scored with 0. The withdrawal threshold was determined as the lower force that elicited more than 50% of positive response and the maximal cut-off was established as 15g.

3.3 Chronic Inflammation Induction

Male Wistar rats (weighing 150-250 g) were anaesthetized with a ketamine and diazepam mixture (2:1 100/5 mg/kg i.p.) and 50 µL of CFA was injected just posterior to the second row of vibrissae. 28 days after induction, rats were sacrificed.

Henceforth, for convenience purposes, the CFA-injected animals will be referred simply as the CFA group.

3.4 Acute Cell Dissociation

3.4.1 Trigeminal Ganglia

Rats were deeply anaesthetized with sodium pentobarbital (100 mg/kg i.p.) and sacrificed by decapitation. After extraction, the ganglia were rapidly dissected in six identical pieces and incubated in cold oxygenated Krebs dissociation solution containing (in mM) 120 NaCl, 5 KCl, 20 PIPES, 1 $CaCl_2$, 1 $MgCl_2$, 25 glucose (pH 7.4, NaOH) with 2 mg/mL collagenase type IV (Gibco, cat. no. 17104-019) for 45 minutes at 32ºC. To mechanically triturate the ganglia and to dissociate the neurones, fire-polished Pasteur pipettes were used 20 minutes into and by the end of the incubation. After this period, 2 mg/mL trypsin (Sigma, cat. no. T9201) was added to the preparation which was incubated for another 40 minutes at 32ºC. To conclude the dissociation, after an additional mechanical trituration step, the cell suspension was centrifuged for 5 minutes at 1500 rpm and the resulting pellet was resuspended in 2 mL of Krebs dissociation solution.

The dissociated cells were maintained at room temperature until plated on Petri dishes precoated with poly-L-lysine (Sigma, cat. no. P4707) to be used in electrophysiological experiments between 30 minutes and 8 hours after the dissociation.

3.4.2 Dorsal Root Ganglia

Rats were sacrificed as mentioned previously, and the L4-L6 lumbar DRGs were dissected as described by Serrão 2015 and Szwarc 2017. The harvested ganglia were sectioned into four equal pieces in cold oxygenated Krebs dissociation solution and incubated for 50 minutes at 32ºC with 3 mg/mL collagenase type IA (Sigma, cat no. C9891). The DRG pieces were mechanically dissociated with fire-polished Pasteur pipettes 25 minutes into and by the end of the incubation. After this period, 2,5 mg/mL trypsin (Sigma, cat. no. T9201) was added and the preparation was incubated for another 45 minutes at 32ºC. To conclude the dissociation, after an additional mechanical trituration step, the cell suspension was centrifuged for 5 minutes at 2000 rpm and the resulting pellet was resuspended in 2 mL of Krebs dissociation solution.

3.5 WHOLE-CELL VOLTAGE CLAMP

Dissociated neurones were plated in poly-L-lysine coated plates with external solution containing (in mM): NaCl 140; KCl 4; CaCl2 1; MgCl2 1.5; HEPES 10; Glucose 15 (pH 7.4, NaOH; 305 mOsm) at room temperature. Isolated small neurones (15-20 µm) were selected for patch-clamp recordings. The size interval selection was based on measurements of 927 isolated TG neurons. These results (not shown) revealed that the cell body sizes are divided in three groups, of which the range 15-20 µm was the smallest. It is presumed that those correspond to the C-fibres, the subject of the present work.

Membrane currents were recorded with an electrometer (Axon Instruments, Axopatch 200B), an analogue/digital signal converter (Axon Instruments, DigiData 1200) and Clampex 6.0.3 (Axon Instruments) software.

Microelectrodes (2-3MΩ) were pulled from borosilicate glass (Science Products GmbH®, GB150T-8P) and filled with an internal solution containing (in mM): KF 140; MgCl2 1; Na1/2-HEPES 10; EGTA 10; CaCl2 1; Na2ATP 2; Na-GTP 0.5 (pH 7.2–7.3, KOH; 290 mOsm).

After gigaohm seal formation and membrane disruption, a holding potential of -70 mV was set and transients were set to zero. Currents were measured with capacitance compensation and series resistance compensation (85%), filtered at 10kHz, sampled at 5kHz, using a Digidata 1200 AC converter.

The voltage dependence of activation was studied by applying 1040 ms long command pulses varying from -80 to +50 mV in 10 mV increments preceded by a 120 ms long hyperpolarizing prepulse to -120 mV. On the other hand, in order to evaluate the potential at which the channels inactivate (voltage dependence of inactivation), a 600 ms long command pulse to +10 mV was elicited preceded by a 1040 ms prepulse varying from -140 to +10 mV.

3.5.1 Data Analysis

The electrophysiology data were analysed with Clampfit 10.3 (Axon Instruments®) software, Microsoft Excel (Microsoft Office 2016), and Origin Pro 8 (Microcal Software®).

To study the voltage dependence of activation, activation profiles were represented by current (I) as a function of voltage and the resulting curve was used to calculate ionic conductance (G) and current density (J). Conductance was obtained by applying Equation 3.1 where V_m represents the pulse voltage and E_K stands for the K^+ equilibrium potential calculated by Nernst equation.

$$G = \frac{I}{V_m - E_K}$$

Equation 3.1

Conductance values were then normalised to the maximal amplitude and fitted with a Boltzmann equation (Equation 3.2) in which $V_{1/2}$ is the membrane potential that elicits activation of half the channel population and V_S is the slope factor.

$$G/G_{max} = \frac{A_1 - A_2}{1 + e^{V_{1/2} - V_m/V_s}} + A_2$$

Equation 3.2

To analyse the voltage dependence of inactivation, currents were normalised to the maximal amplitude (I/I_{max}) and plotted as a function of prepulse potential. The resulting data points were then fitted with a sum of sigmoid functions (Equation 3.3) where $V_{1/2\ fast}$ and $V_{1/2\ slow}$ are the half-activation potentials of the fast and slow components of steady-state inactivation of K^+ currents and $V_{S\ fast}$ and $V_{S\ slow}$ are the corresponding slopes.

$$I/I_{max} = \frac{A_1}{1 + e^{(V_{1/2\ fast} - Vm)/V_{S\ fast}}} + \frac{1 - A_1}{1 + e^{(V_{1/2\ slow} - Vm)/V_{S\ slow}}}$$

Equation 3.3

In order to be able to draw comparisons between cells, current density (J) was calculated by multiplying the current (I) by the whole-cell capacitance (C) (Equation 3.4). Capacitance is a measure of the cell's ability to store charge and is proportional to the cell size and it is considered that cell membranes have a capacitance of 1 μF/cm^2 [68].

$$J = I \times C$$

Equation 3.4

3.6 PHARMACOLOGICAL EXPERIMENTS

In order to assess the contribution of $K_V1.3$ on the currents obtained from small-diameter TG neuron, experiments with PAP-1 (Santa Cruz Biotechnology, cat no. 870653-45-5), a specific blocker of this channel [69], were performed. Only cells displayed a stable current profile were used.

The final concentration of PAP-1 in the external solution was 2 nM, a concentration at which this molecule only blocks $K_V1.3$ [69]. A stock solution of PAP-1 was made with DMSO at a concentration of 1 mM. After dilution, the DMSO concentration in the perfusing solution was 0.002%, a concentration that had no effect in small-diameter DRG neurones (unpublished data).

3.7 STATISTICAL ANALYSIS

Statistical analysis was performed with SigmaStat 3.5 (Systat Software Inc®). After testing the data for normality and equal variance, appropriate tests were applied: Student's t-test was used as a parametric test and Mann-Whitney test was the chosen non-parametric test. Differences were considered significant when $p < 0.05$. Results are presented as mean ± S.E.M. (standard error of the mean).

4 RESULTS

4.1 BEHAVIOURAL TESTING

During the course of the model no exacerbated stress reactions were observed: weight gain was similar between CFA rats and the control group and there were no signs of excessive scratching such as hair loss or superficial injury to the whisker pad. As mentioned, two types of behaviours were evaluated: spontaneous behaviour and mechanical sensitivity, assessed by the withdrawal threshold.

4.1.1 Spontaneous Behaviour

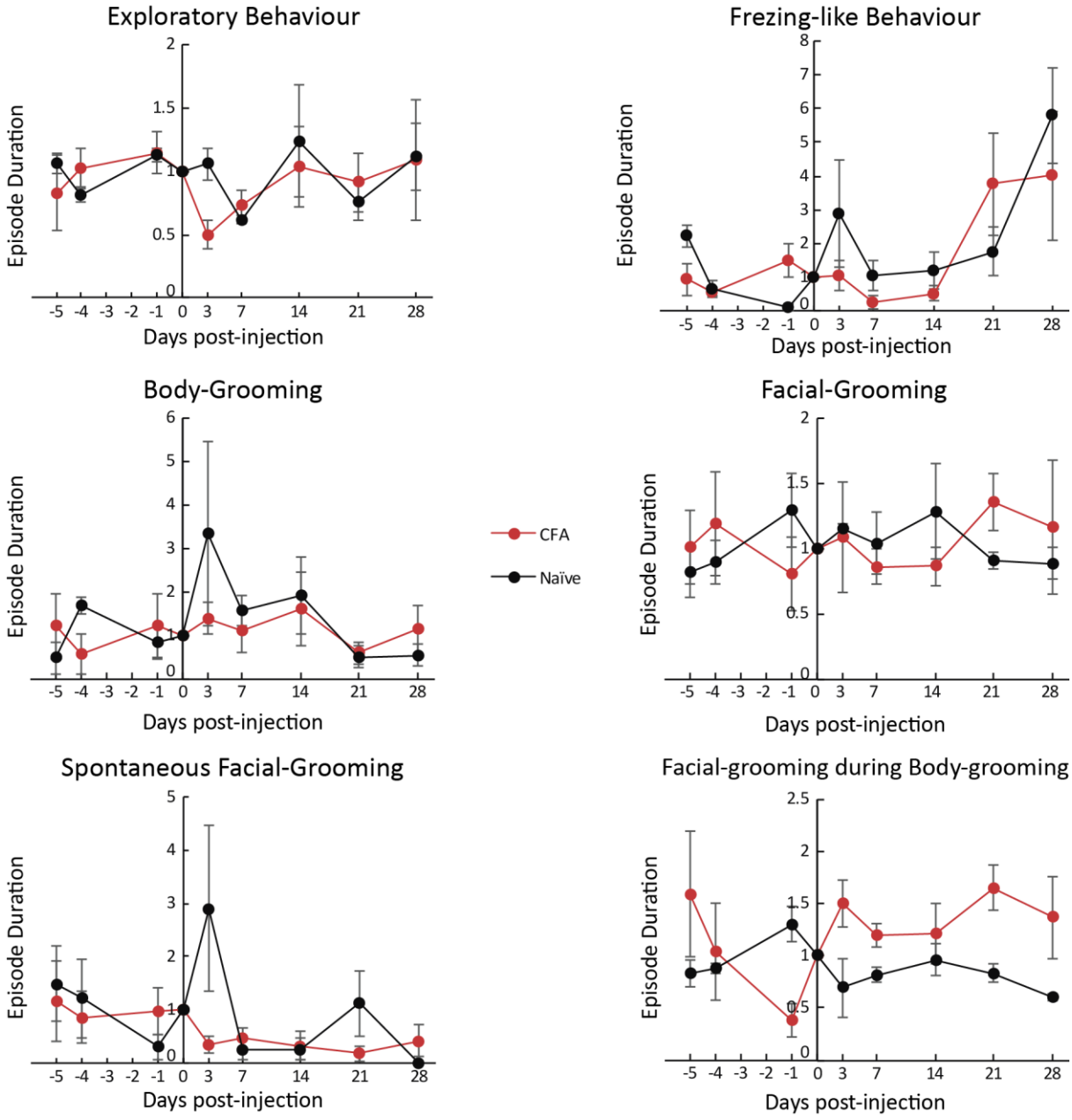

Figure 4.1 **Mean episode duration of the studied non-evoked behaviours.**
Changes in behavioural activity were evaluated through the normalised duration of six behavioural categories both for naïve (black, n=3) and CFA-injected (red, n=3) rats. No clear tendency was observed in either one of these behavioural categories (Mann-Whitney test, $p > 0.005$). For clarity purposes, the time scale used differs between the pre- and the post-injection periods. Error bars represent S.E.M.

As far as the evaluated non-evoked behaviours were concerned, no significant differences were observed (Figure 4.1, Mann-Whitney test, $p > 0.005$). However, the duration of the face-grooming episodes performed during body-grooming displays an increase in the CFA-treated animals that is, nonetheless, not significant (Figure 4.1, Mann-Whitney test, $p > 0.005$). Moreover, asymmetric face-grooming, an established sign of nociceptive disturbance [27], was only observed in one CFA-injected animal at the 28th day post-injection (data not shown).

4.1.2 Mechanical Sensitivity

Comparing the Ipsilateral whisker-pad (injected) with the Contralateral one (internal control), the head withdrawal thresholds of the CFA-injected rats were significantly reduced (Figure 4.2 A; Mann-Whitney test, $p < 0.005$). On the other hand, no changes were observed in the Naïve group (Mann-Whitney test, $p > 0.005$).

Two rats, one of each group (Naïve and CFA), became hyporesponsive 14 days after model induction and therefore their data are not included. As the 14th day post-injection coincided with building work in the rodent facility and both groups were equally affected, it can be assumed that the lack of response was due to external factors. Nevertheless, the hyporesponsive CFA-injected rat was used for electrophysiological experiments since it performed asymmetric face-grooming and its behavioural cues were indicative of pain (see discussion) [27].

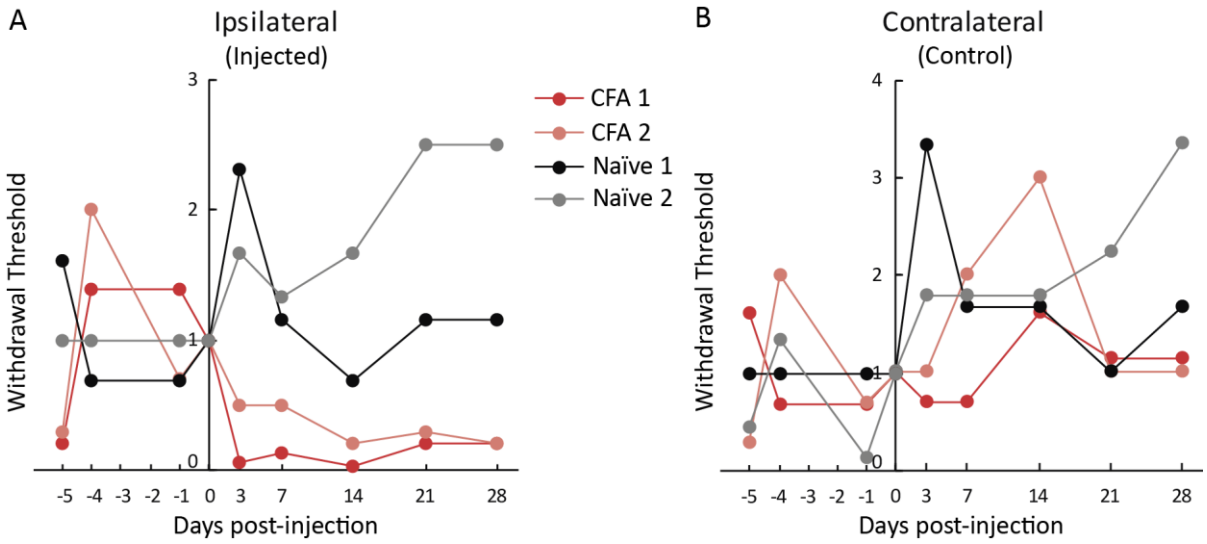

Figure 4.2 **Withdrawal Threshold**.
Comparing the pre-injection thresholds to the post-injection values, CFA injection leads to a significant decrease of the withdrawal threshold (Mann-Whitney test, $p < 0.005$). The changes observed in the contralateral side (internal control) are not significant (Mann-Whitney test, $p > 0.005$). Due to the small sample, the data from each rat is presented separately.

4.2 Electrophysiology

4.2.1 K^+ Currents in Small-Diameter Trigeminal Ganglion Neurones

Figure 4.3 shows the average K^+ current elicited by a +50 mV pulse preceded by a -120 mV prepulse of n = 34 cells obtained from N = 11 rats. These currents are characterised by two current components as the total current is better fit with a sum of two exponential functions. The I_{Fast} component, corresponding to the I_A is characterised by a fast inactivation rate (Figure 4.3, lighter blue; $\tau = 50{,}96 \pm 3{,}91$ ms). On the other hand, the I_{Slow} component that comprises I_K, I_D, and I_M and has a slower inactivation (Figure 4.3, darker blue; $\tau = 266{,}5 \pm 1653$ ms).

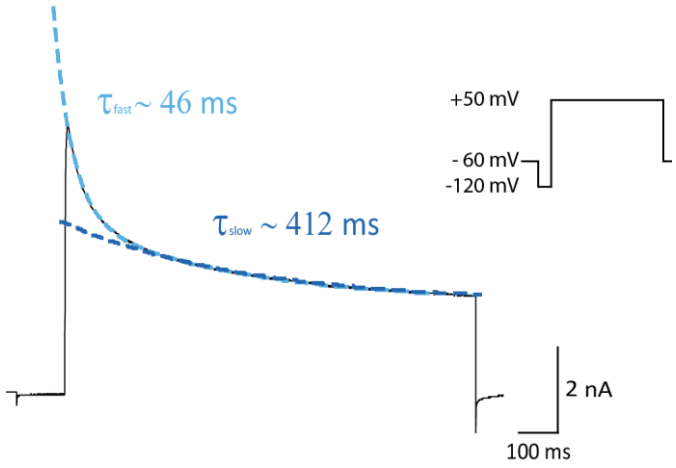

Figure 4.3 **Whole-cell K^+ current in a small-diameter TG neuron.**
The trace represents the average (n = 34) K^+ current elicited when a 50 mV pulse preceded by a -120 mV prepulse was applied to small-diameter TG neurones. This current is better fit with a double exponential function characterised by an initially faster inactivation rate (lighter blue; τ = 50,96 ± 3,91) followed by slower one (darker blue; τ = 266,5 ± 1653). Each of these inactivation rates defines a current component: I_{Fast} and I_{Slow}, respectively.

The cells from naïve animals studied can be divided into two populations (Figure 4.4): while 76% of the cells (n = 26) have a modest expression of the I_{Fast} component (Figure 4.4 A), a sub-group of 23% (n = 8) of the small-diameter TG neurones show a current profile dominated by the fast-inactivating component (Figure 4.4 B).

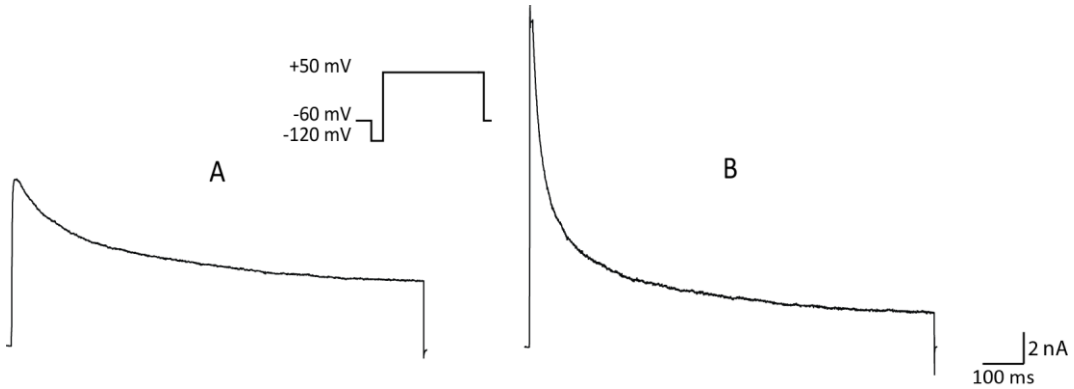

Figure 4.4 **Typical K^+ current traces of two major types of voltage clamp recordings observed in small-diameter TG neurones.**
A – Most small-diameter TG neurones (76%; n= 26) showed a modest expression of I_{Fast}; B – In fewer cases (24%; n=8) the fast-inactivating component has a stronger expression. Currents were elicited by a 50 mV pulse preceded by a -120 mV prepulse

4.2.1.1 Voltage-Dependence of Activation

The voltage-dependence of activation was studied as previously mentioned (see inset in Figure 4.5). Figure 4.5 shows the average currents elicited by application of such voltage protocol, recorded from n = 34 cells obtained from N = 11 naïve rats.

Conductance was calculated for each voltage applied, the G/V relationship was normalised and fit with a Boltzmann equation, as described in the methods section (Figure 4.6 A). As mentioned, the $V_{1/2}$ values correspond to the Vm value for which half the channels are active, and V_S is the slope factor, an indication of how the conductance varies with the voltage. While the I_{Fast} component has a $V_{1/2}$ value of -8,76 ± 1,96 mV, and a V_S of 14,86 ± 1,05 mV, the I_{Slow} component is characterised by a $V_{1/2}$ of -3,34 ± 1,59 mV, and a V_S = 18,06 ± 0,95 mV. Hence, I_{Slow} is slightly more sensitive to voltage than the I_{Fast} component.

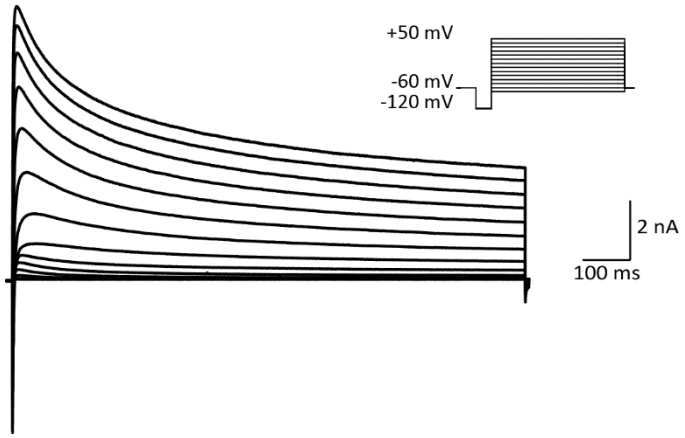

Figure 4.5 **Activation profile of K^+ currents in small-diameter TG neurones.**
Averaged (n = 34) K^+ currents obtained from small-diameter TG neurones in response to a pulse varying from -80 to +50 mV in 10 mV increments preceded by a -120 mV prepulse

The voltage dependence of the current kinetics was also studied (Figure 4.6 B). For that purpose, the inactivation time constants of each component were calculated and plotted against the Vm values (Figure 4.6 B). The kinetics of both current components show dependence on voltage and there was a tendency for faster inactivation rate in response to increasing Vm values. The τ_{Fast} values ranged from 50.96 to 69.83 while the τ_{Slow} was between 351.93 and 424.44 ms.

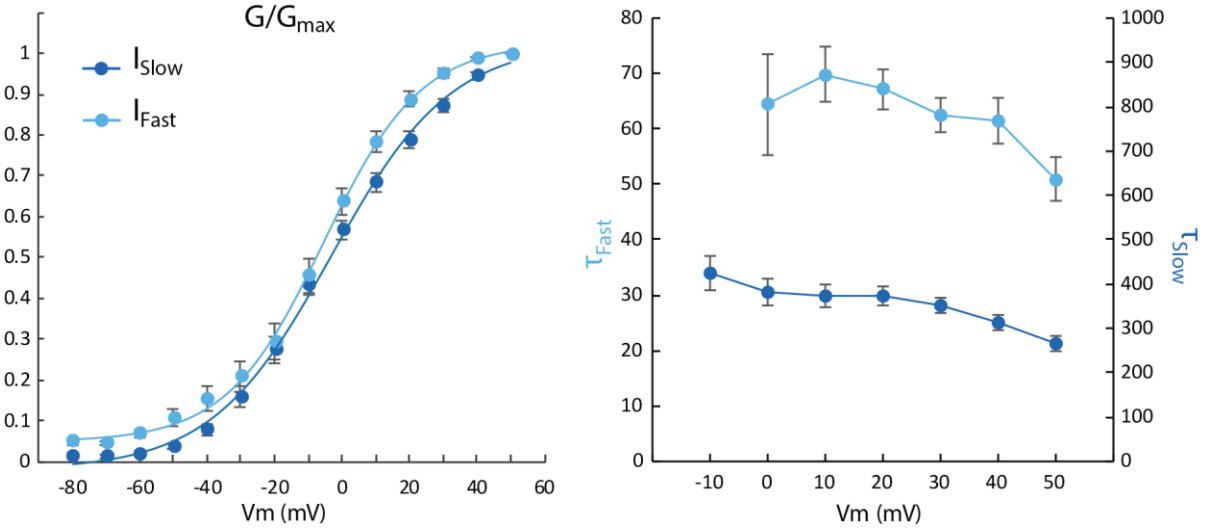

Figure 4.6 **Voltage dependence of activation and Voltage dependence of kinetics.**
A: Relationship between conductance and voltage and the matching Boltzmann functions.
B: Variation of the current components kinetics.

4.2.1.2 Voltage-Dependence of Inactivation

The voltage-dependence of inactivation was studied as previously described. Figure 4.7 shows the average currents elicited by the voltage protocol illustrated in the figure inset, recorded from n = 29 cells obtained from N = 11 naïve rats (Figure 4.7 A), the normalization of each current component to its maximum and the double Boltzmann equation with which the data were fit (Figure 4.7 B).

The fact that the inactivation curve was better fit with a double Boltzmann function means that there are two terms, each characterised by a different set of parameters. The expression of the more depolarized term, is not consistent enough for a well-defined fit, interfering with its use in the consequent analysis. However, the $V_{1/2}$ of this is estimated to be approximately -30 to -20 mV.

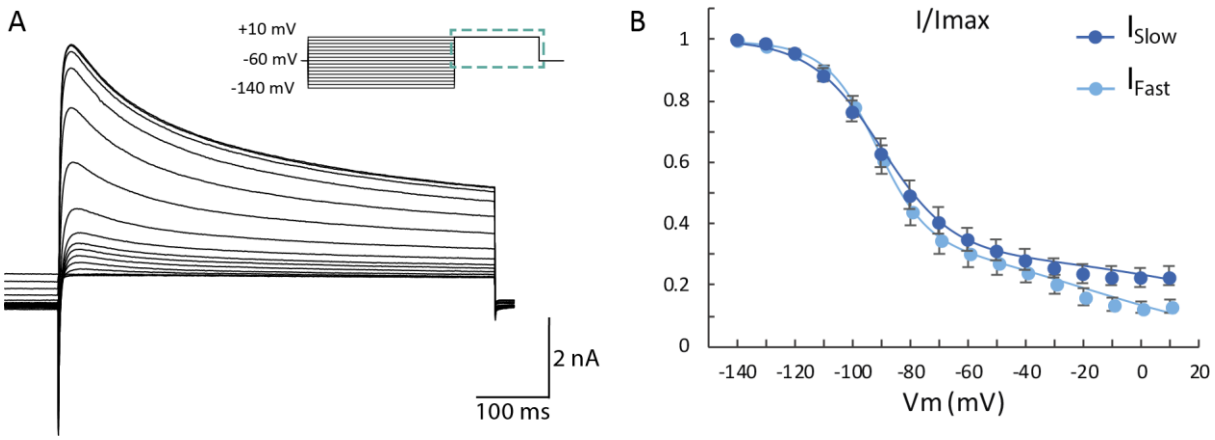

Figure 4.7 **Voltage dependence of inactivation**
A: Average (n = 29) K_V currents obtained from small-diameter TG neurones in response to a +10 mV pulse preceded by a prepulse varying from -140 to +10 mV in 10 mV increments; B: Relationship between the normalised current and the Vm and corresponding double Boltzmann function.

For the more hyperpolarized term of the inactivation profile, the $V_{1/2}$ values of the I_{Fast} and I_{Slow} components are -89,84 ± 2,32 mV and -88,83 ± 1,75 mV, respectively. Both the I_{Slow} and the I_{Fast} components have similar V_S values in this term: -10,61 ± 2,35 mV for the I_{Fast} component, and -10,79 ± 0,39 mV for the I_{Slow} component.

4.2.2 K+ Currents in a Model of Chronic Orofacial Pain

4.2.2.1 Voltage-Dependence of Activation

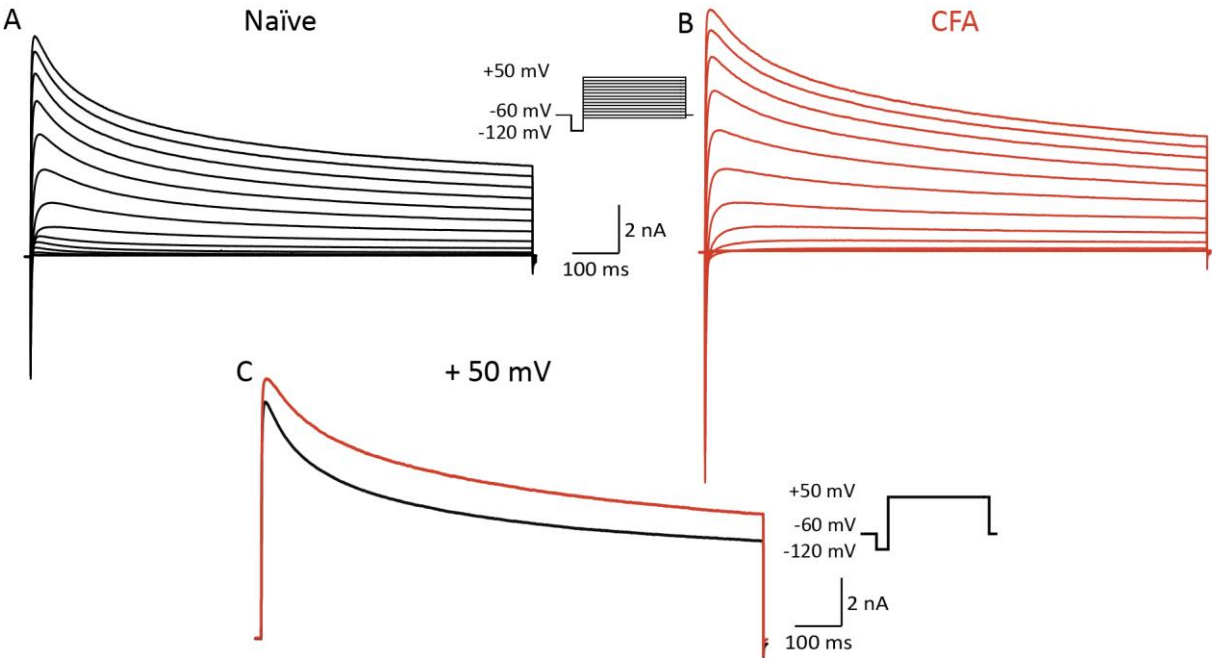

Figure 4.8 **Changes in the activation profile.**
A and B: Average Naïve (A, black; n = 34) and CFA (B, red; n = 16) K_V currents obtained in response to a pulse varying from -80 to +50 mV in 10 mV increments preceded by a -120 mV prepulse.
C: Superposition of the average currents obtained in response to the +50 mV pulse recorded from Naïve (black; n = 34) and CFA (red; n = 16) cells.

In this study, n=16 cells of N = 3 CFA-injected rats were characterised and compared to the n = 34 cells from N = 11 naïve rats previously described. Figure 4.8 shows the average activation currents

of these cells (Figure 4.8 B) next to the average naïve currents (Figure 4.8 A). Comparing the currents elicited by a +50 mV depolarizing pulse preceded by a -120 mV prepulse (Figure 4.8 C), the CFA group appears to have increased current amplitudes as well as an enhanced I_{Slow} component. However, comparing the actual values of current density (Figure 4.9) no significant differences were detected. Nonetheless, in the smaller sample that constitutes the CFA group, there is a set of outliers whose current density is considerably higher (Figure 4.9 B and D). As such cells are not present in the Naïve group, their presence in the CFA treated rats is suggestive that some fibres may be more extensively affected.

As far as the current kinetics is concerned (Figure 4.10), differences were observed in the inactivation rate of the I_{Slow} component (Figure 4.10 B). This already slowly inactivating component becomes even slower in the CFA model. This change allied to the fact I_{Slow} to some extent enhanced means that for the CFA model there is a larger current-charge for K^+ currents. As this current component is essential for membrane repolarization, such alterations could have an impact on the shape of the action potential and/or firing rate.

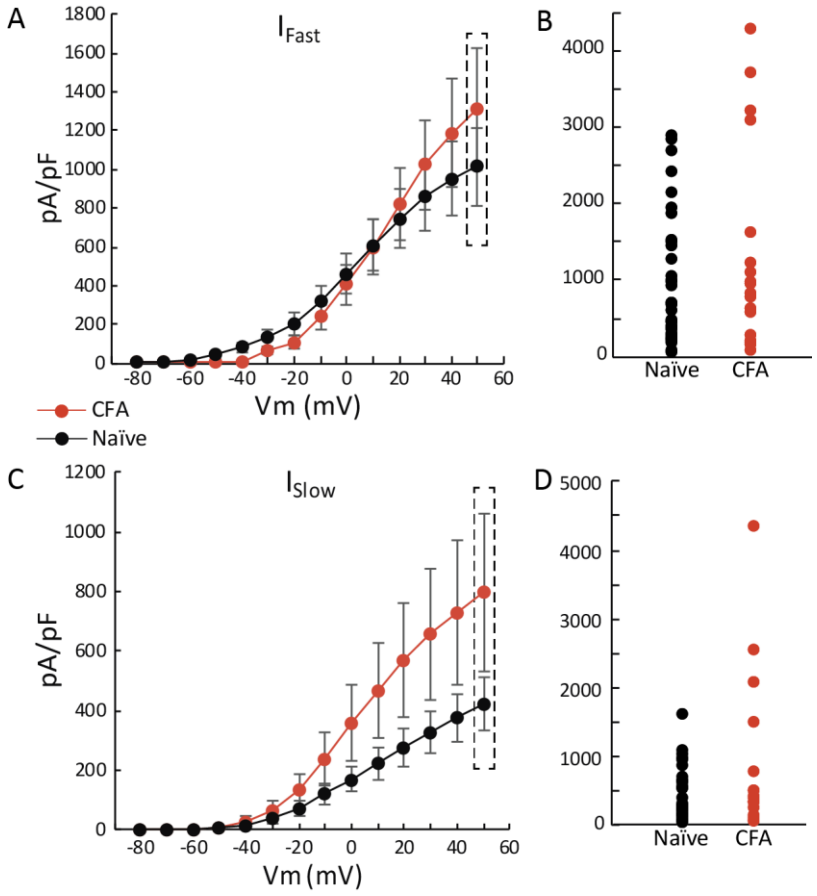

Figure 4.9 **Changes in current density.**
The A and C panels show how current density changes depending on the Vm values (Average values ± S.E.M.). Despite the lack of statistically significant differences, as shown in B and D (50 mV data points), the CFA group had a few outliers which can be noteworthy as the sample size is considerably smaller (n = 34 for the naïve group versus n = 16 for the CFA group).

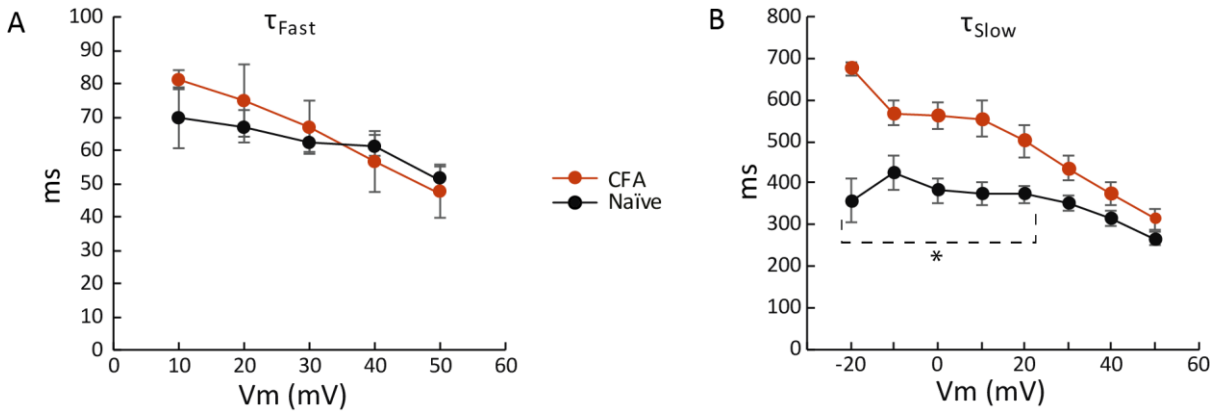

Figure 4.10 **Changes in the voltage dependence of kinetics.**
A - Rate of inactivation of the I_{Fast} component (τ_{Fast}); B - Rate of inactivation of the I_{Slow} component (τ_{Slow})
While τ_{Fast} seems to remain unaltered, for most of the voltages the I_{Slow} component inactivates at a slower rate in CFA-injected rats compared to the Naïve group ($p < 0,05$; t-test).

Regarding the voltage dependence of activation (Figure 4.11), looking at the normalised conductance and corresponding Boltzmann equation, while the I_{Slow} component shows similar parameters in both conditions ($V_{1/2}$ of -3,34 ± 1,59 mV for Naïve, and -5,40 ± 2,12 mV for CFA; V_S of 18,06 ± 0,95 mV for Naïve, and 15,50 ± 1,10 mV for CFA), there are significant differences in the values for the I_{Fast} component. The $V_{1/2}$ value went from -8,76 ± 1,96 mV in the Naïve condition to -0,56 ± 2,07 mV in the CFA model. This difference ($p<0.005$, t-test) means that the K_V channels activate at more depolarized Vm values in the pain condition. The V_S values were also altered: 14,86 ± 1,05 mV for Naïve and 11,61 ± 0,65 mV for CFA ($p<0.005$, t-test) which means that the slope is steeper in the CFA condition and therefore conductance is less dependent on voltage.

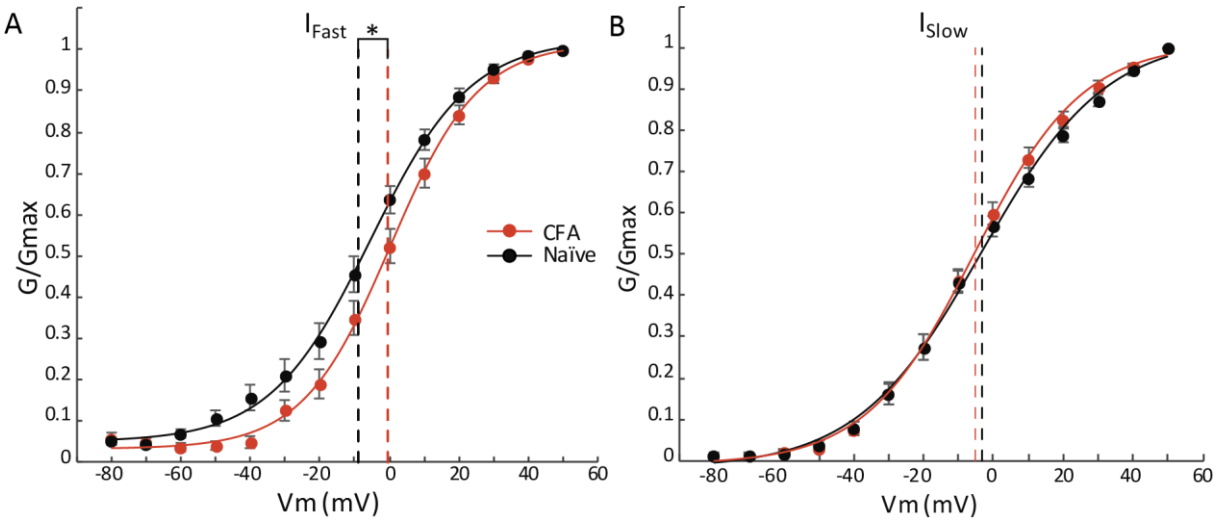

Figure 4.11 **Changes in the voltage dependence of activation**.
A – I_{Fast} component; B – I_{Slow} component.
K^+ currents of small-diameter TG neurones of CFA-treated animals activate at more depolarized membrane potentials as indicated by the difference in the $V_{1/2}$ values of the I_{Fast} component ($p < 0,05$; t-test)

4.2.2.2 Voltage-Dependence of Inactivation

To analyse the voltage-dependence of inactivation n = 14 cells obtained from N = 3 CFA-injected rats were studied (Figure 4.12 A) and compared to the to the n = 29 cells from N = 11 naïve rats previously described (Figure 4.12 B).

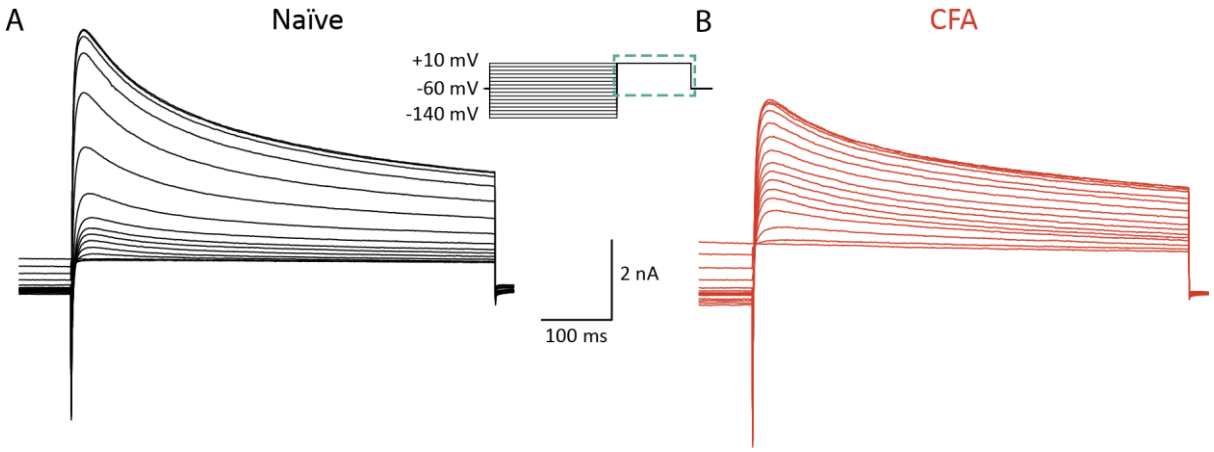

Figure 4.12 **Changes in the inactivation profile**.
Average Naïve (A, black; n = 29) and CFA (B, red; n = 14) K_V currents obtained from small-diameter TG neurones in response to a +10 mV pulse preceded by a prepulse varying from -140 to +10 mV.

Contrasting with the voltage dependence of activation, it was in the I_{Slow} component inactivation curve that the changes were more clear (Figure 4.13 and Table 4.1).

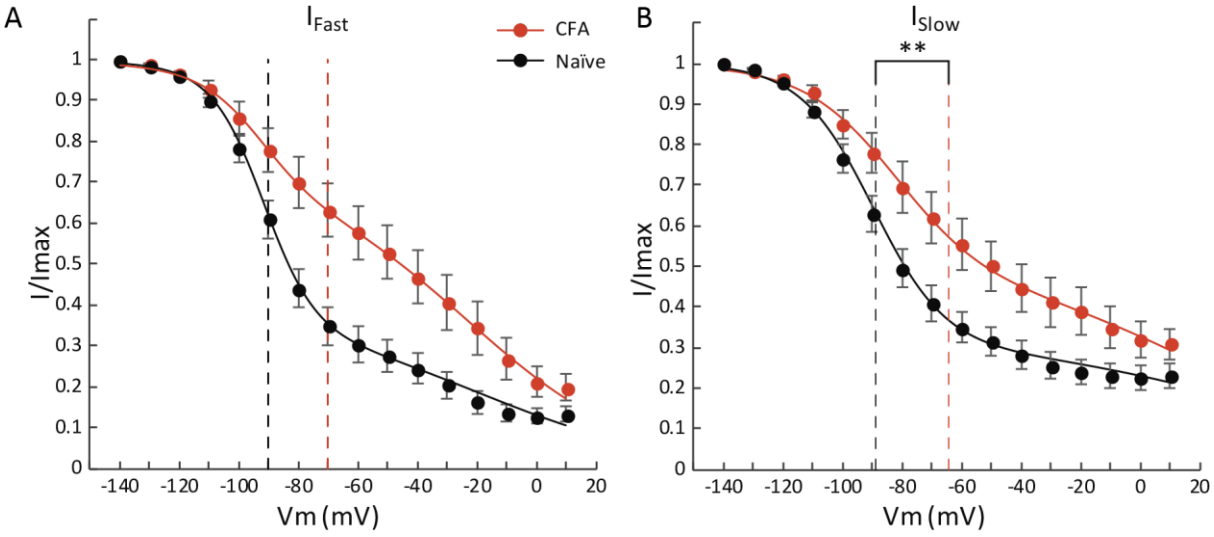

Figure 4.13 **Changes in the voltage dependence of inactivation**.
A – I_{Fast} component; B – I_{Slow} component.
K^+ currents from small-diameter TG neurones obtained from CFA-treated animals inactivate at more depolarized Vm values as their $V_{1/2}$ values are higher ($p < 0{,}001$; t-test).

Both inactivation curves shifted to the right as the $V_{1/2}$ became more depolarized but the difference was only significant in the I_{Slow} component. This means that the K_V channels inactivate at more depolarized Vm values, implying that more channels are active, or available for activation during the AP. In other words, in the context of chronic pain, the K_V channel inactivation is impaired which is consistent with the results obtained from the study of the inactivation kinetics (Figure 4.10 B).

Table 4.1 **Double Boltzmann fitting parameters for the inactivation profile of both components.**
The inactivation profiles of both current components became depolarized, a difference that was only significant for the I_{Slow} component.

		Naïve	**CFA**	
I_{Fast} component	$V_{1/2}$	-89,84 ± 2,32 mV	-70,10 ± 7,86 mV	NS; t-test
	V_S	-11,48 ± 9,37 mV	-3,28 ± 17,21 mV	NS; t-test
		Naïve	**CFA**	
I_{Slow} component	$V_{1/2}$	-88,83 ± 1,75 mV	-64,21 ± 9,27 mV	p<0,001; t-test
	V_S	-10,79 ± 0,39 mV	-11,58 ± 1,84 mV	NS; t-test

4.2.3 K^+ Currents in Small-Diameter Sensory Neurones

Since the trigeminal system has distinct symptomatic responses to injury and inflammation when compared to its spinal counterparts, the DRG [8,9], and considering the importance of the later in pain research, the different K_V current components characterised in TG neurones were compared them to those obtained from DRG neurones.

4.2.3.1 Voltage-Dependence of Activation

For this comparison n = 12 DRG cells of N = 7 naïve rats were characterised (Figure 4.14 B) and compared to the n = 34 TG cells from N = 11 naïve rats previously described (Figure 4.14 A).

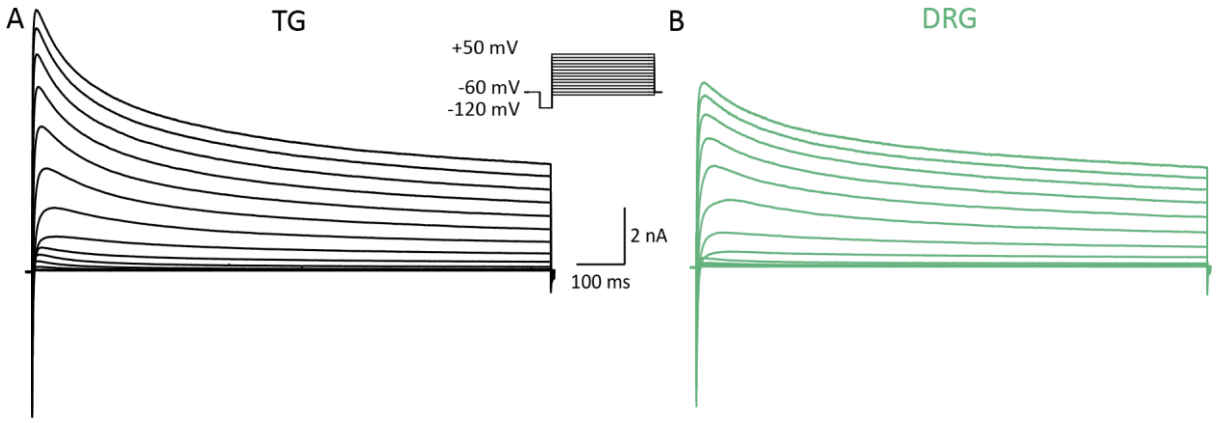

Figure 4.14. **Activation profile of K^+ currents in small-diameter sensory neurones.**
Average TG (A, black; n = 34) and DRG (B, green; n = 16) K_V currents obtained in response to a 50 mV pulse preceded by a -120 mV prepulse.

The nature of the current traces is generally similar (Figure 4.14) and the most visible disparity is the apparent higher current amplitude on TG neurones. However, this difference becomes diluted when normalised to the whole-cell capacitance (current density, Figure 4.15).

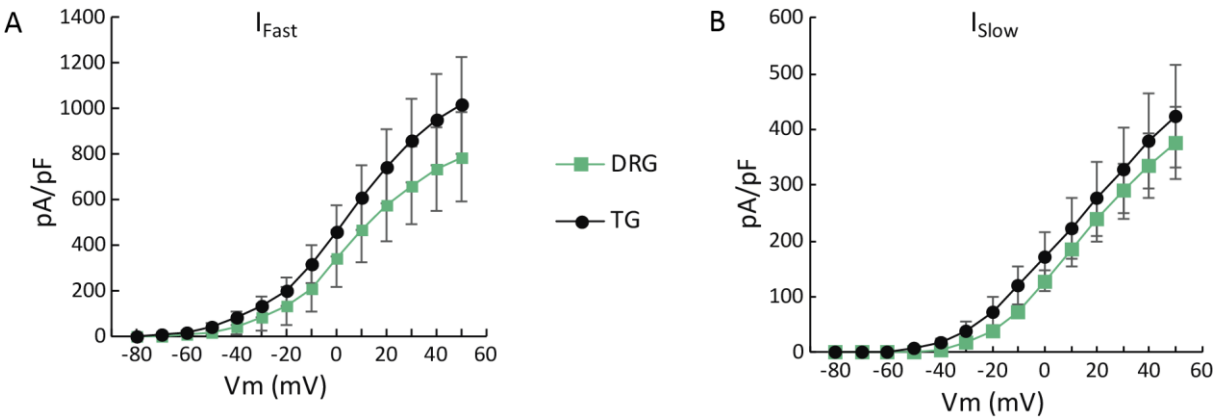

Figure 4.15 **Current density of K^+ currents in small-diameter sensory neurones from TG (black) and DRG (green).**
A – I_{Fast} component; B – I_{Slow} component.
No significant differences were found between small-diameter sensory neurones.

Conductance was once again calculated for each voltage and the normalised G/V curve was fit with Boltzmann functions (Figure 4.16) whose fitting parameters are presented in Table 4.2.

The only difference observed was in the V_S value of the I_{Slow} component: 18,06 ± 0,95 mV for TG and 14,62 ± 1,30 mV for DRG ($p<0,005$; t-test). This means that the slope of the Boltzmann function that fits the TG data is steeper and therefore, the K^+ channel activation is somehow less dependent on voltage.

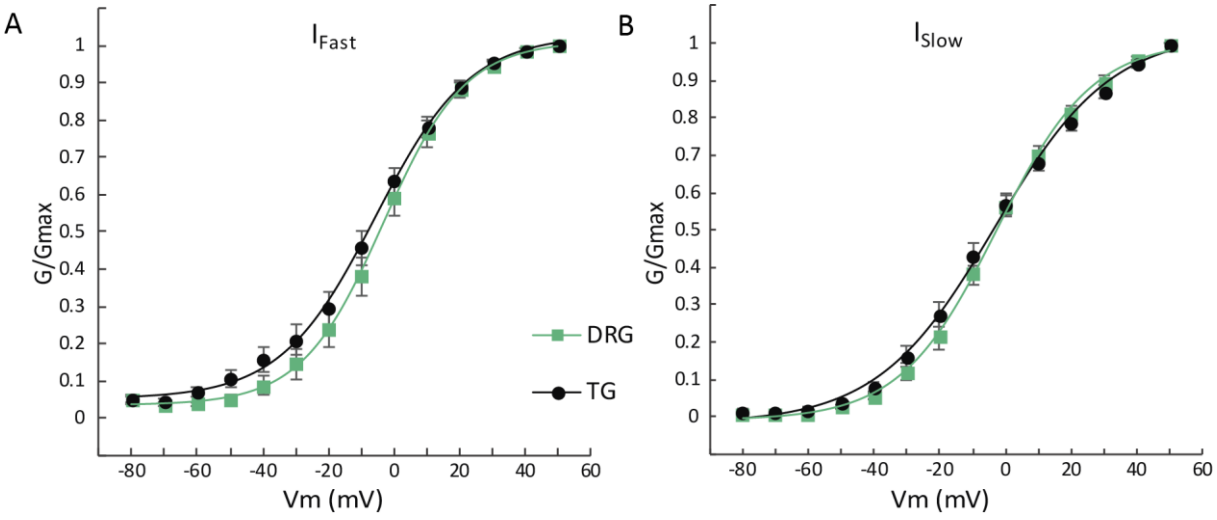

Figure 4.16 **Voltage dependence of activation of K^+ currents in small-diameter sensory neurones from TG (black) and DRG (green).**
A – I_{Fast} component; B – I_{Slow} component.
Overall small-diameter neurones from both TG and DRG show a similar voltage dependence of activation profile.

Table 4.2 **Boltzmann fitting parameters of the activation curves.**
The activation profiles of both TG and DRG neurones were similar with the exception of the V_S value of the I_{Slow} component.

		TG	**DRG**	
I_{Fast} component	$V_{1/2}$	-8,76 ± 1,96	-3,52 ± 2,98	NS; t-test
	V_S	14,86 ± 1,05	11,49 ±1,45	NS; t-test
I_{Slow} component	$V_{1/2}$	-3,34 ± 1,59 mV	-2,85 ± 2,13 mV	NS; t-test
	V_S	18,06 ± 0,95 mV	14,62 ± 1,30 mV	$p<0,005$; t-test

4.2.3.2 Voltage-Dependence of Inactivation

To analyse the voltage-dependence of inactivation n = 12 DRG cells obtained from N = 7 naïve rats were studied (Figure 4.17 B) and compared to the n = 29 cells from N = 11 naïve rats described in previous sections (Figure 4.17 A).

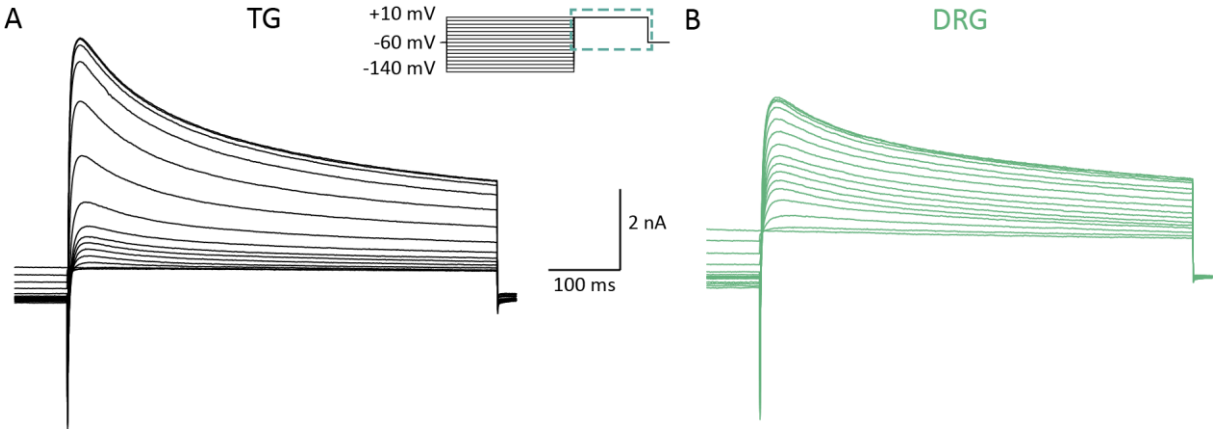

Figure 4.17 **Inactivation profile of K^+ currents in small-diameter sensory neurones.**
Average TG (A, black; n = 29) and DRG (B, green; n = 12) K_V currents obtained in response to a +10 mV pulse preceded by a prepulse varying from -140 to +10 mV

The global observation of the inactivation curves (Figure 4.17) leads to similar inferences as the activation profiles since the current amplitudes seem to be higher in small-diameter TG neurones.

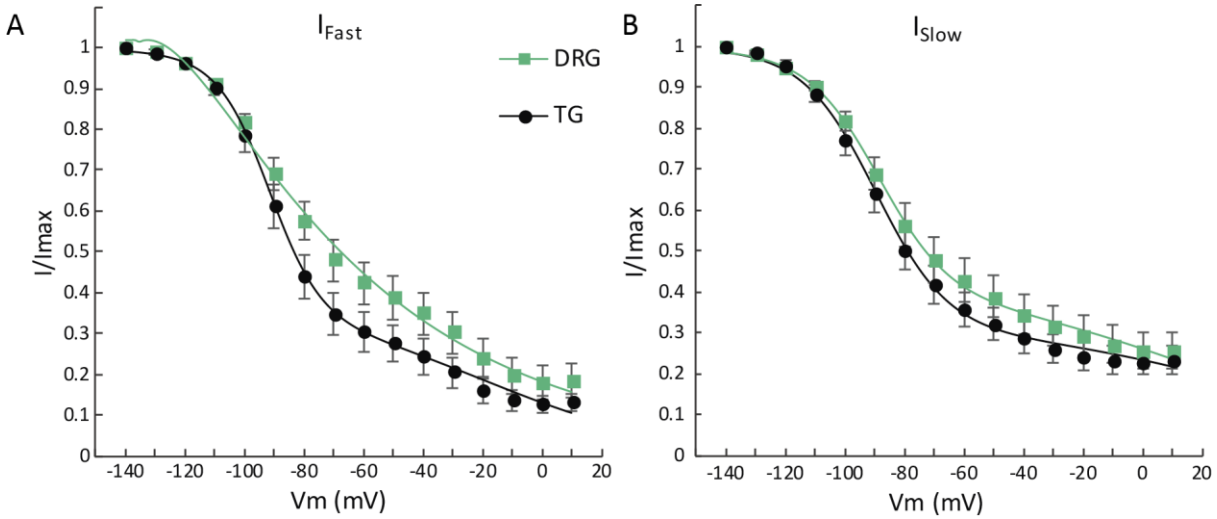

Figure 4.18 **Voltage dependence of inactivation of K^+ currents in small-diameter sensory neurones from TG (black) and DRG (green).**
A – I_{Fast} component; B – I_{Slow} component.

Nevertheless, no significant differences were observed between the fitting parameters for both current components (Table 4.3).

Table 4.3 **Double Boltzmann fitting parameters for the inactivation profile of small-diameter sensory neurones.** No significant differences were found between the inactivation profiles of TG and DRG.

		Naïve	**DRG**	
I_{Fast} Component	$V_{1/2}$	-89,84 ± 2,32 mV	-89,83 ± 2,61 mV	NS; t-test
	V_S	-11,48 ± 9,37 mV	-9,57 ± 1,25 mV	NS; t-test
		Naïve	**DRG**	
I_{Slow} Component	$V_{1/2}$	-88,83 ± 1,75 mV	-84,90 ± 3,33 mV	NS; t-test
	V_S	-10,79 ± 0,39 mV	15,95 ± 7,79 mV	NS; t-test

4.3 PHARMACOLOGICAL EXPERIMENTS

The subtraction between CFA and naïve K^+ currents (data not shown) and the suggestive results from previous work carried on the DRG [67] indicate that $K_V1.3$ could not only be functionally expressed in the TG but also underlie the changes observed in the chronic pain condition. To further investigate this hypothesis, the effect of a specific $K_V1.3$ blocker (PAP-1) on the whole-cell K^+ currents from small-diameter TG neurones was explored.

The application of a concentration of 2 nM of PAP-1 produced an effect on the current kinetics. The current kinetics suffered alterations as the I_{Slow} component inactivation rate (τ_{Slow}) went from 400.98 ± 49.77 ms to 195.02 ± 42.36 ms ($p<0,05$; t-test). On the other hand, the I_{Fast} component inactivation rate (τ_{Fast}) showed no significant changes (38.46 ± 12.85 ms before, and 21.97 ± 5.18 ms after PAP-1 application).

The current trace resulting from the subtraction of the remaining current from the total is shown in Figure 4.19 (B). The kinetics observed match the $K_V1.3$ profile [59,70] implying that this K_V subunit, whose expression in the TG has been confirmed [71], forms functional channels in small-diameter TG neurones.

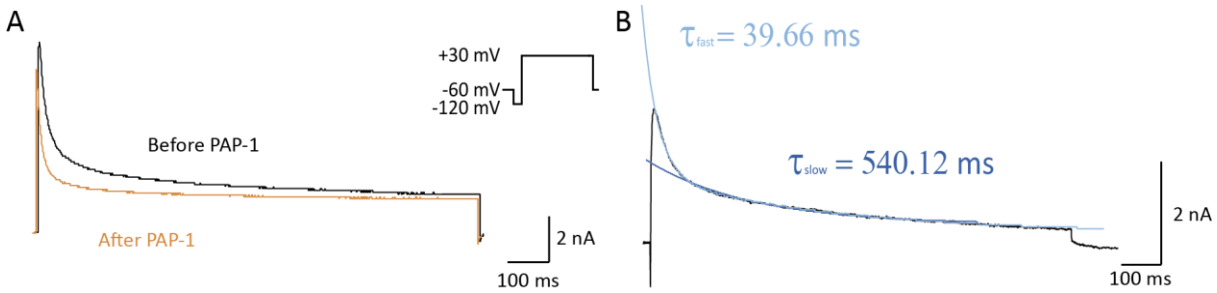

Figure 4.19 **Effect of PAP-1 (2nM) on small-diameter TG neurones.**
A: Average traces (n=5) for total current (black) and current remaining after PAP-1 application (orange). Traces represent currents elicited by a +30 mV depolarizing pulse preceded by a -120 mV prepulse.
B: Subtraction of the remaining current after PAP-1 application from the total current. Average trace (n=5) obtained in response to a +30 mV depolarizing pulse preceded by a -120 mV prepulse and respective inactivation rates.

5 DISCUSSION

5.1 CFA-INDUCED CHRONIC INFLAMMATORY HYPERALGESIA

Most inflammatory pain models performed in the orofacial region are maintained for a maximum of 14 days [23,49,50,53,54]. Notwithstanding there are indications that the injection of CFA into the whisker pad results in an inflammatory response that produces hyperalgesia that lasts up to 28 days as demonstrated by the work of Morgan and colleagues in which the expression of Na_V channels was

studied [52]. In the present work, the model used by Morgan et al. was used to study how chronic inflammatory pain changes the K^+ currents of small-diameter TG neurones.

5.1.1 Spontaneous Behaviour

Overall the behavioural categories studied here show no significant changes after CFA injection (Figure 4.1) with the noteworthy exception of face-grooming during body-grooming (BF) tending to have longer episodes after CFA injection.

Despite these results, it would be imprudent to conclude that the nociceptive mechanisms remain unaltered. The behavioural testing procedure was largely based on experiments whose focuses were neuropathic pain [27,28,38] and since nerve injury causes a more intense sensory disturbance [18], it is possible that the milder effects of inflammation were overlooked. In fact, personal observations indicate that the most visible change was not in the time spent performing each behavioural category but how the episodes were distributed through the testing time, a variable that was not evaluated in the present work. As CFA-injected rats tend to perform face-grooming actions in bursts and become less active earlier than naïve animals, future experiments will include an analysis of the time course of such patterns rather than relying solely on the study of average episode duration.

5.1.2 Mechanical Sensitivity

The CFA injection to the whisker pad led to a reduction of the withdrawal threshold that remained stable for at least 28 days (Figure 4.2). Although only two of the three rats injected showed this response, the presence of asymmetric face-grooming and the general apathy displayed during the test procedure suggest that the third injected animal was subject to sensory disturbance.

The assessment of the mechanical sensitivity was one of the biggest challenges during the model establishment. For this particular measurement, the habituation period is crucial as the stimulated area is very susceptible to novel stimuli. Restraining the animals using a towel allows a clear view of the region to be stimulated and of the contact between the von Frey filament and the skin so the correct stimulus application can be ensured. Moreover, these conditions enable some degree of freedom of movement of the upper body which not only allows for normal withdrawal responses to be performed but also reduces stress. Although not entirely stress-free, compared to methods using specialised restraining devices, using a towel is easier and more versatile while having similar advantages.

The persistence of behavioural signs of pain for 28 days implies a crucial difference between the orofacial region and the hind paw since a single CFA-injection causes hyperalgesia only up to 2 weeks in knee joint models [66,67,72]. This may be a result of not only the higher mechanical sensitivity of the orofacial region but also the larger relative volume of CFA injected.

5.2 INFLAMMATION-INDUCED CHANGES IN K^+ CURRENTS

The biophysical properties of K_V currents obtained from naïve small-diameter TG neurones in this study are similar to control currents found in the literature [33,42,43,49].

As K^+ currents are responsible for the membrane repolarization, they have an important role in the suppression of action potential generation, control of the firing rate and firing pattern. Thus, these currents are, to some degree, responsible reducing neuron excitability and therefore, increased neuronal excitability should be linked to a decreased K_V channel activity. However, the present results suggest that 28 days following CFA-injection to the whisker pad, K^+ currents from small-diameter TG neurones are instead potentiated. In fact, the results presented in this dissertation are in apparent disagreement with the conclusions of Takeda and colleagues [49] who report that two days after CFA injection into the TMJ total peak K^+ current density was significantly reduced.

With pain chronicity, there is an increase in the excitatory sodium current (I_{Na}) which will inevitably promote a more intensified AP generation and excitability in general [73]. The maintenance of this exacerbated neuronal performance for a long period may require the readjustment of homeostatic mechanisms. Hence, to accommodate the prolonged repetitive firing expected in affected neurones during chronic pain, an increase in the K^+ currents may be necessary in order to balance the increased I_{Na}. In the absence of this regulation nerve failure and even cell death may ensue probably via impaired toxic intracellular calcium dynamics.

Furthermore, after 28 days of chronic response, it is likely that not only the peripheral nervous system but also the central mechanisms are sensitized. Specifically, for such a prolonged response to be viable throughout the entire pathway, the ionic channels must adjust their activity in order to accommodate a more frequent and intense activity. This is supported by the changes observed in the current kinetics such as the slower I_{Slow} component observed in the CFA model (Figure 4.10). Since this component is crucial for the repolarization phase, its slower activation results in longer APs, a change that leads to an augmented transmitter release in the central terminal contributing to central sensitization (Figure 1.3). Also related with a possible longer AP, is the depolarized activation $V_{1/2}$ value for I_{Fast} component (Figure 4.11), as this faster component controls the duration of the depolarization phase.

The depolarizing shift observed in the inactivation curves of the pain model neurones, significant only for I_{Slow} (Figure 4.13 and Table 4.1) is also related to the promotion of repolarization. This deviation implies that there are less inactive channels at the resting membrane potential, i.e. more channels are ready to be activated. Once again this is an unexpected result that goes against the changes reported by Takeda et al. [49] and may represent a plastic change allowing the accommodation of repetitive firing in a long-term context. A recurrent result in chronic pain studies is the inhibition of I_A [33,42,43,67], a result that was not visible in this work. However, the increased I_{Slow} component may conceal this effect as both components contribute for the initial portion of the current studied.

Other than the already discussed difference in the time course of the pain-related behavioural changes, no significant differences between TG and DRG neurones were found at the electrophysiological level. These similarities are extended to the distinct neuronal subpopulations found (Figure 4.4). A higher I_A expression has been described in "peptidergic" small-diameter DRG neurones in comparison with "non-peptidergic" fibres [74] which is consistent with both the present findings and the presence of the characteristic neurochemical profiles that has been demonstrated in the TG [75]. Furthermore, the augmented contribution of I_{Slow} detected in the present work coincide with results obtained in small-diameter DRG neurones following CCI of the sciatic nerve [67]. Thus, despite the anatomical and symptomatic differences, the pain transduction and sensitization pathways appear to be similar in both body regions. These results suggest a common therapeutic approach may be explored since a drug that whose target is involved in these mechanisms may have a dual application.

5.3 $K_V1.3$: A POTENTIAL TARGET

Taking into account the slow nature of the current component affected by pain suggested that the underlying channels could be $K_V1.1$, 1.2, 1.3 or 1.6. Considering that $K_V1.3$ mediates a slow inactivating current [59,70] and that it was previously implicated in the pathophysiology of chronic neuropathic pain [67,76], we set up to further investigate this channel. The experiments using a specific $K_V1.3$ blocker, PAP-1, confirmed that this subunit not only is present in small-diameter TG neurones but also forms functional channels. However, the involvement of other subunits should not be rejected since the correlation between current components and specific subunits is not straight-forward due to the possible heterotetrameric channel structure.

These results will be considered in future work that will explore how the $K_V1.3$-mediated currents are altered in the orofacial CFA model.

6 CONCLUSIONS

In the present work, an orofacial pain model was successfully established and changes in the K_V-mediated currents were detected. It was determined that a single CFA injection to the whisker pad leads to an inflammatory response responsible for hyperalgesic behaviours lasting up to 28 days. After such period, in the context of animal models, pain can be considered chronic.

The study of K_V currents in neurones from the chronic pain condition revealed an apparent inconsistency with what would be expected in a hyperexcitable state since the currents underlying the membrane repolarization seem to be potentiated. This modulation allows for a prolonged repetitive firing pattern to be sustainable without leading to nerve failure. Additionally, the observed changes also hint to a modified AP shape that will be reflected in the release of neurotransmitters in the central terminal of the nociceptors and thus may be involved in the establishment of central sensitization.

In conclusion, in the context of chronic orofacial pain, K_V currents are likely involved in mechanisms responsible for inducing central sensitization. Furthermore, in the long-term, these currents undergo changes that allow the frequent firing by maintaining the crucial equilibrium between excitation and repolarization.

6.1 FUTURE DIRECTIONS

The present work represents a pilot experiment and therefore further studies must be carried out as the sample size is still very limited and many questions remain unanswered.

As stated, the evaluation of spontaneous pain is of paramount importance in any chronic pain study. Due to the natural complexity of animal behaviour, this goal was not quite achieved. Hopefully, in the future, an even more thorough and complex analysis of the behavioural readouts will provide more valuable results.

Even though the voltage protocols applied and solutions used were not designed to isolate Na^+ currents, an increase in the inward currents is visible (Figure 4.8). Such currents will be further studied in following experiments in an effort to clarify how the various ion channels involved are affected. Furthermore, the hypothesized changes at the action potential level will be tested with resort to current-clamp experiments.

As the whole ganglion was used, it is expected that many of the studied neurones correspond to branches other than the ION which innervates the whisker pad (Figure 1.6). Therefore, the outlier group in the CFA-treated ganglia with a tendency to higher current densities may account for directly affected fibres. For rectifying this issue, a neuronal marker will be used in future studies allowing to identify the cell bodies that innervate the target area.

As evidenced by the results of the pharmacological experiments, $K_V1.3$ is present in small-diameter TG neurones. Taking into account results previously obtained in the lab [67], future work will also be focused on the role of this channel and the currents it mediates and how they change in the context of chronic orofacial pain.

7 REFERENCES

1. Melzack, R. & Casey, K. L. Sensory, Motivational, and Central Control Determinants of Pain. *Ski. senses* 423–439 (1968).
2. Reichling, D. B., Green, P. G. & Levine, J. D. The fundamental unit of pain is the cell. *Pain* **154,** (2013).
3. Julius, D. & Basbaum, A. I. Molecular mechanisms of nociception. *Nature* **413,** 203–210 (2001).
4. Basbaum, A. I., Bautista, D. M., Scherrer, G. & Julius, D. Cellular and Molecular Mechanisms of Pain. *Cell* **139,** 267–284 (2009).
5. Du, X. & Gamper, N. Potassium channels in peripheral pain pathways: expression, function and therapeutic potential. *Curr. Neuropharmacol.* **11,** 621–40 (2013).
6. Schaible, H. G. in *Analgesia* 3–28 (Springer Berlin Heidelberg, 2007). doi:10.1007/978-3-540-33823-9_1
7. Woolf, C. J. & Ma, Q. Nociceptors—Noxious Stimulus Detectors. *Neuron* **55,** 353–364 (2007).
8. Takeda, M., Matsumoto, S., Sessle, B. J., Shinoda, M. & Iwata, K. Peripheral and Central Mechanisms of Trigeminal Neuropathic and Inflammatory Pain. *J. Oral Biosci.* **53,** 318–329 (2011).
9. Fried, K., Bongenhielm, U., Boissonade, F. M. & Robinson, P. P. Nerve injury-induced pain in the trigeminal system. *Neuroscientist* **7,** 155–165 (2001).
10. Woolf, C. J. & Costigan, M. Transcriptional and posttranslational plasticity and the generation of inflammatory pain. *Proc. Natl. Acad. Sci.* **96,** 7723–7730 (1999).
11. Sun, W. H. & Chen, C. C. Roles of Proton-Sensing Receptors in the Transition from Acute to Chronic Pain. *J. Dent. Res.* **95,** 135–142 (2016).
12. Vaughn, A. H. & Gold, M. S. Ionic Mechanisms Underlying Inflammatory Mediator-Induced Sensitization of Dural Afferents. *J. Neurosci.* **30,** 7878–7888 (2010).
13. Woolf, C. J. Neuronal Plasticity: Increasing the Gain in Pain. *Science (80-.).* **288,** 1765–1768 (2000).
14. IASP. Classification of chronic pain. Descriptions of chronic pain syndromes and definitions of pain terms. (2011).
15. Azevedo, L. F., Costa-Pereira, A., Mendonça, L., Dias, C. C. & Castro-Lopes, J. M. Epidemiology of chronic pain: A population-based nationwide study on its prevalence, characteristics and associated disability in Portugal. *J. Pain* **13,** 773–783 (2012).
16. Van Hecke, O., Torrance, N. & Smith, B. H. Chronic pain epidemiology and its clinical relevance. *Br. J. Anaesth.* **111,** 13–18 (2013).
17. Bereiter, D. A., Hirata, H. & Hu, J. W. Trigeminal subnucleus caudalis: Beyond homologies with the spinal dorsal horn. *Pain* **88,** 221–224 (2000).
18. Krzyzanowska, A. & Avendaño, C. Behavioral testing in rodent models of orofacial neuropathic and inflammatory pain. *Brain Behav.* **2,** 678–697 (2012).
19. Lazarov, N. E. *Comparative analysis of the chemical neuroanatomy of the mammalian trigeminal ganglion and mesencephalic trigeminal nucleus*. *Progress in Neurobiology* **66,** (2002).
20. Woda, A. *et al.* Towards a new taxonomy of idiopathic orofacial pain. *Pain* **116,** 396–406 (2005).
21. Sessle, B. J. Acute and Chronic Craniofacial Pain: Brainstem Mechanisms of Nociceptive Transmission and Neuroplasticity, and Their Clinical Correlates. *Crit. Rev. Oral Biol. Med.* **11,** 57–91 (2000).
22. Cruccu, G. *et al.* Trigeminal neuralgia: New classification and diagnostic grading for practice and research. *Neurology* **87,** 220–228 (2016).
23. Kuzawinska, O., Lis, K., Cudna, A. & Balkowiec-Iskra, E. Gender differences in the neurochemical response of trigeminal ganglion neurons to peripheral inflammation in mice. *Acta Neurobiol Exp* **74,** 227–

232 (2014).

24. Noseda, R. & Burstein, R. Migraine pathophysiology: Anatomy of the trigeminovascular pathway and associated neurological symptoms, cortical spreading depression, sensitization, and modulation of pain. *Pain* **154,** S44–S53 (2013).

25. Berge, O.-G. Predictive validity of behavioural animal models for chronic pain. *Br. J. Pharmacol.* **164,** 1195–206 (2011).

26. Barrett, J. E. The pain of pain: Challenges of animal behavior models. *Eur. J. Pharmacol.* **753,** 183–190 (2015).

27. Vos, B. P., Hans, G. & Adriaensen, H. Behavioral assessment of facial pain in rats: Face grooming patterns after painful and non-painful sensory disturbances in the territory of the rat's infraorbital nerve. *Pain* **76,** 173–178 (1998).

28. Vos, B. P., Strassman, A. M. & Maciewicz, R. J. Behavioral evidence of trigeminal neuropathic pain following chronic constriction injury to the rat's infraorbital nerve. *J. Neurosci.* **14,** 2708–23 (1994).

29. Bennett, G. J. & Xie, Y.-K. A peripheral mononeuropathy in rat that produces disorders of pain sensation like those seen in man. *Pain* **33,** 87–107 (1988).

30. Flake, N. M. & Gold, M. S. Inflammation alters sodium currents and excitability of temporomandibular joint afferents. *Neurosci. Lett.* **384,** 294–299 (2005).

31. Ahn, D. K. *et al.* Compression of the trigeminal ganglion produces prolonged nociceptive behavior in rats. *Eur. J. Pain* **13,** 568–575 (2009).

32. Ma, F., Zhang, L., Lyons, D. & Westlund, K. N. Orofacial neuropathic pain mouse model induced by Trigeminal Inflammatory Compression (TIC) of the infraorbital nerve. *Mol. Brain* **5,** 44 (2012).

33. Kitagawa, J. *et al.* Mechanisms involved in modulation of trigeminal primary afferent activity in rats with peripheral mononeuropathy. *Eur. J. Neurosci.* **24,** 1976–1986 (2006).

34. Abd-Elsayed, A. A. *et al.* KCNQ channels in nociceptive cold-sensing trigeminal ganglion neurons as therapeutic targets for treating orofacial cold hyperalgesia. *Mol. Pain* **11,** 45 (2015).

35. Liu, C.-Y. *et al.* The role of large-conductance, calcium-activated potassium channels in a rat model of trigeminal neuropathic pain. *Cephalalgia* **35,** 16–35 (2015).

36. Vit, J.-P., Jasmin, L., Bhargava, A. & Ohara, P. T. Satellite glial cells in the trigeminal ganglion as a determinant of orofacial neuropathic pain. *Neuron Glia Biol.* **2,** 247 (2006).

37. Benoliel, R., Eliav, E. & Tal, M. No sympathetic nerve sprouting in rat trigeminal ganglion following painful and non-painful infraorbital nerve neuropathy. *Neurosci. Lett.* **297,** 151–154 (2001).

38. Ding, W. *et al.* An Improved Rodent Model of Trigeminal Neuropathic Pain by Unilateral Chronic Constriction Injury of Distal Infraorbital Nerve. *J. Pain* (2017). doi:10.1016/j.jpain.2017.02.427

39. Luiz, A. P., Kopach, O., Santana-Varela, S. & Wood, J. N. The role of Nav1.9 channel in the development of neuropathic orofacial pain associated with trigeminal neuralgia. *Mol. Pain* **11,** 72 (2015).

40. Pozza, D. H., Castro-Lopes, J. M., Neto, F. L. & Avelino, A. Spared nerve injury model to study orofacial pain. *Indian J. Med. Res.* **143,** 297 (2016).

41. Xu, M., Aita, M. & Chavkin, C. Partial Infraorbital Nerve Ligation as a Model of Trigeminal Nerve Injury in the Mouse: Behavioral, Neural, and Glial Reactions. *J. Pain* **9,** 1036–1048 (2008).

42. Nakagawa, K. *et al.* Alteration of primary afferent activity following inferior alveolar nerve transection in rats. *Mol. Pain* **6,** 9 (2010).

43. Tsuboi, Y. *et al.* Alteration of the second branch of the trigeminal nerve activity following inferior alveolar nerve transection in rats. *Pain* **111,** 323–334 (2004).

44. Davies, S. L. *et al.* Changes in sodium channel expression following trigeminal nerve injury. *Exp. Neurol.* **202,** 207–216 (2006).

45. Bongenhielm, U. & Robinson, P. P. Spontaneous and mechanically evoked afferent activity originating from myelinated fibres in ferret inferior alveolar nerve neuromas. *Pain* **67,** 399–406 (1996).

46. Bongenhielm, U. *et al.* Expression of sodium channel SNS/PN3 and ankyrin(G) mRNAs in the trigeminal ganglion after inferior alveolar nerve injury in the rat. *Exp. Neurol.* **164,** 384–395 (2000).

47. Eriksson, J. *et al.* Behavioral changes and trigeminal ganglion sodium channel regulation in an orofacial neuropathic pain model. *Pain* **119,** 82–94 (2005).

48. Seino, H., Seo, K., Maeda, T. & Someya, G. Behavioural and histological observations of sensory impairment caused by tight ligation of the trigeminal nerve in mice. *J. Neurosci. Methods* **181,** 67–72 (2009).

49. Takeda, M. *et al.* Enhanced excitability of rat trigeminal root ganglion neurons via decrease in A-type potassium currents following temporomandibular joint inflammation. *Neuroscience* **138,** 621–630 (2006).

50. Takeda, M. *et al.* Temporomandibular joint inflammation potentiates the excitability of trigeminal root ganglion neurons innervating the facial skin in rats. *J. Neurophysiol.* **93,** 2723–2738 (2005).

51. Takeda, M., Tanimoto, T., Nasu, M. & Matsumoto, S. Temporomandibular joint inflammation decreases the voltage-gated K+ channel subtype 1.4-immunoreactivity of trigeminal ganglion neurons in rats. *Eur. J. Pain* **12,** 189–195 (2008).

52. Morgan, J. R. & Gebhart, G. F. Characterization of a Model of Chronic Orofacial Hyperalgesia in the Rat: Contribution of NAV 1.8. *J. Pain* **9,** 522–531 (2008).

53. Imbe, H. *et al.* Orofacial Deep and Cutaneous Tissue Inflammation and Trigeminal Neuronal Activation. *Cells Tissues Organs* **169,** 238–247 (2001).

54. Benoliel, R., Wilensky, A., Tal, M. & Eliav, E. Application of a pro-inflammatory agent to the orbital portion of the rat infraorbital nerve induces changes indicative of ongoing trigeminal pain. *Pain* **99,** 567–578 (2002).

55. Mogil, J. S. Animal models of pain: progress and challenges. *Nat. Rev. Neurosci.* **10,** 283–294 (2009).

56. Mogil, J. S., Davis, K. D. & Derbyshire, S. W. The necessity of animal models in pain research. *Pain* **151,** 12–17 (2010).

57. Hille, B. *Ion channels of excitable membranes*. *Sunderland Massachusetts USA* (Sinauer Sunderland, MA, 2001).

58. Armstrong, C. M. Voltage-Gated K Channels. *Sci. Signal.* **2003,** re10-re10 (2003).

59. Coetzee, W. A. *et al.* Molecular diversity of K+ channels. *Ann. N. Y. Acad. Sci.* **868,** 233–285 (1999).

60. Grizel, A. V., Glukhov, G. S. & Sokolova, O. S. Mechanisms of activation of voltage-gated potassium channels. *Acta Naturae* **6,** 10–26 (2014).

61. Stühmer, W. *et al.* Molecular basis of functional diversity of voltage-gated potassium channels in mammalian brain. *EMBO J.* **8,** 3235–3244 (1989).

62. Horn, R. How ion channels sense membrane potential. *Proc. Natl. Acad. Sci. U. S. A.* **102,** 4929–4930 (2005).

63. Tsantoulas, C. & McMahon, S. B. Opening paths to novel analgesics: The role of potassium channels in chronic pain. *Trends Neurosci.* **37,** 146–158 (2014).

64. Tsantoulas, C. Emerging potassium channel targets for the treatment of pain. *Curr. Opin. Support. Palliat. Care* 1 (2015). doi:10.1097/SPC.0000000000000131

65. Pongs, O. Voltage-gated potassium channels: From hyperexcitability to excitement. *FEBS Lett.* **452,** 31–35 (1999).

66. Serrão, J. M. M. Validation of voltage-gated sodium channels from dorsal root ganglia neurons as a pharmacological target for the treatment of Chronic pain. (Faculdade de Ciências da Universidade de Lisboa, 2015).

67. Szwarc, B. Characterization of Voltage-Gated Potassium Channels from Dorsal Root Ganglia Neurons in Neuropathic and Inflammatory Chronic Pain. (Faculdade de Ciências da Universidade de Lisboa, 2017).

68. Molecular Devices. The Axon Guide. **94,** 1078–82 (2010).

69. Schmitz, A. & Sankaranarayanan, A. Design of PAP-1, a selective small molecule Kv1. 3 blocker, for the suppression of effector memory T cells in autoimmune diseases. *Mol. Pharmacol.* **68,** 1254–1270 (2005).

70. Grissmer, S. *et al.* Pharmacological characterization of five cloned voltage-gated K+ channels, types Kv1.1, 1.2, 1.3, 1.5, and 3.1, stably expressed in mammalian cell lines. *Mol. Pharmacol.* **45,** 1227–34 (1994).

71. Liu, L. & Simon, S. A. Modulation of IA Currents by Capsaicin in Rat Trigeminal Ganglion Neurons. *J. Neurophysiol.* **89,** 1387–1401 (2003).

72. Ren, K. & Dubner, R. Inflammatory Models of Pain and Hyperalgesia. *ILAR J.* **40,** 111–118 (1999).

73. Bagal, S. K. *et al.* Recent progress in sodium channel modulators for pain. *Bioorganic Med. Chem. Lett.* **24,** 3690–3699 (2014).

74. Vydyanathan, A. A-Type Voltage-Gated K+ Currents Influence Firing Properties of Isolectin B4-Positive But Not Isolectin B4-Negative Primary Sensory Neurons. *J. Neurophysiol.* **93,** 3401–3409 (2005).

75. Triner, J. C. Defining neurochemical properties and functions of primary sensory neurons in the rat trigeminal ganglion. (2013).

76. Yang, E.-K., Takimoto, K., Hayashi, Y., de Groat, W. C. & Yoshimura, N. Altered expression of potassium channel subunit mRNA and alpha-dendrotoxin sensitivity of potassium currents in rat dorsal root ganglion neurons after axotomy. *Neuroscience* **123,** 867–74 (2004).